

Research Article

Revealing the Mineralogical and Petrographic Signs of Fluid-Related Processes in the Kelebia Basement Area (Szeged Basin, S Hungary): A Case Study of Alpine Prograde Metamorphism in a Permo-Triassic Succession

Andrea Varga , Elemér Pál-Molnár, and Béla Raucsik

Department of Mineralogy, Geochemistry and Petrology, University of Szeged, Szeged H-6722, Hungary

Correspondence should be addressed to Andrea Varga; raucsikvarga@geo.u-szeged.hu

Received 19 August 2022; Revised 23 December 2022; Accepted 10 January 2023; Published 25 January 2023

Academic Editor: Martina Zucchi

Copyright © 2023 Andrea Varga et al. This is an open access article distributed under the Creative Commons Attribution License, which permits unrestricted use, distribution, and reproduction in any medium, provided the original work is properly cited.

The Szeged Basin (S Hungary) occupies a relatively central position within the European Alpine–Carpathian–Dinaride orogenic belt. An ongoing controversy about the tectonic position of the study area indicates that its evolution is still not fully understood; however, several important hydrocarbon occurrences are known in the fractured basement reservoirs. The main aim of this contribution is to investigate the petrographic features and possible Alpine metamorphic conditions of volcanic/volcanoclastic and siliciclastic rocks from the Kelebia basement area. Due to the outcrop conditions and poor exposure, study samples are obtained from cores and core chips resulting from oil exploration. Based on an evaluation of petrographic (including also cathodoluminescence analysis) and microstructural features, joined with mineralogical and metamorphic data such as “illite crystallinity” and K-white mica crystallite size obtained by X-ray powder diffractometry (XRPD), a very low- to low-grade (ca. 300°C) Alpine metamorphic imprint of this portion of the basement can be proposed. Several deformation characteristics (deformation lamellae in quartz, deformation twins in dolomite, fragmented porphyroclasts, and strain shadows) were recognized in the studied samples, showing a weakly to moderately developed disjunctive foliation in the Permian rocks, as well as quartz veinlets, microcracks, and fluid inclusion planes in the Lower Triassic sandstones. Most likely, one of the Cretaceous orogenic events, namely, the “Turonian” phase (Early–Late Cretaceous nappe stacking), resulted in the prograde greenschist facies metamorphism in the study area, instead of the burial depth. We propose that the Permo-Triassic cover succession was also affected by shearing episodes accompanied by fluid migrations along the contact zone between the tectonic units. The scientific approach and dataset provided here are examples of how the application of XRPD parameters of phyllosilicates and micropetrographic observations can help to understand the evolution of an orogen and improve knowledge about the basement structure.

1. Introduction

The European Alpine–Carpathian–Dinaride (ACD) orogenic belt was the focus of several relevant projects that resulted in advanced concepts for the tectonometamorphic and thermal evolution of the region (e.g., [1–10]). Furthermore, correlational studies led to improved versions of the tectonic map of the ACD orogenic system [11–17]. In this overall compressional setting, a large rift-related extensional basin, namely, the Pannonian Basin in eastern Central Europe, has developed from the Oligocene

[1–4]. As an integral part of the ACD orogenic system, the back-arc Pannonian Basin is superimposed on two distinct tectonic megaunits or composite terranes with complex internal structures (e.g., [3, 7, 11, 14–17]): (i) the so-called ALCAPA (Alpine–West Carpathian–Pannonian) and (ii) the Tisza–Dacia (Figure 1(a)).

The study area, corresponding to the Codru Nappe System (Figure 1(b)), occupies a relatively central position within the ACD orogenic system; however, its crystalline basement and Permo-Mesozoic cover rocks are largely

covered by thick Cenozoic sedimentary sequences (up to ~7000 m, average thickness: 2000–3000 m) (Figure 1(a)). Isolated basement outcrops are known in the surrounding small hills and mountains (Mecsek and Villány Hills in Hungary, the Slavonian Mts in Croatia, and the northern Apuseni Mts in Romania) (e.g., [5, 6, 16, 17]). Therefore, local to subregional correlations between the main tectonic units are difficult and are generally based on distinct subsurface maps [12, 14, 17], necessarily having uncertainties, assumptions, and tentative interpretations. An ongoing controversy about the tectonic position of the study area (Figure 1(b)) indicates that the Alpine evolution of the central part of the ACD orogenic system is still not fully understood. One reason for this uncertainty is the fact that the pre-Cenozoic basement areas, especially the siliciclastic Permian and Triassic cover formations, are still poorly studied in terms of their timing and petrological characterization. The lack of comprehensive lithostratigraphic and diagenetic/metamorphic control, consequently the scarcity of basement rock samples from the exploration wells, is also one of the important limiting factors.

During the periodic hydrocarbon (HC) exploration projects, it was beyond the scope of the reports to discuss the internal structure of the basement from a pure geological point of view. Standard thin sections with cover glass were prepared from selected basement core samples; however, detailed mineralogical and petrographic data are not available on these rocks. The principal aim of this contribution is to provide a mineralogical and petrological characterization of the Permo-Triassic noncarbonate cover succession in the Kelebia basement area, Szeged Basin. Regarding this study area, the key results together with a compilation of literature data can lead to a better understanding of the tectonic evolution and Alpine structure of the pre-Cenozoic basement and allow for further constraints on the ACD orogenic system.

2. Materials and Methods

2.1. Geological Setting. The Szeged Basin is a subbasin on the southern margin of the Pannonian Basin in Hungary (Figure 1(a)). Within it, the pre-Cenozoic basement belongs structurally to the Tisza megaunit (Tisia Composite Terrane, as referred elsewhere [11, 18]), which traditionally comprises four main nappe systems of Alpine origin formed in the Albian to Turonian (from bottom to top): Mecsek, Bihar, Codru, and Biharia [3, 14–16, 19]. In the Hungarian part of the Tisza megaunit, the Mecsek, Bihar (Villány–Bihar), and Codru (Békés–Codru) Nappe Systems are only found [14–16, 19–21]. The Mecsek and Bihar tectonic units generally consist of a Variscan metamorphic basement intruded by Carboniferous granitoids, as well as Permo-Mesozoic volcanic and sedimentary cover, whereas the Codru Nappe System predominantly consists of nonmetamorphic Permo-Mesozoic rocks of variable thickness which are locally preserved. In the Biharia Nappe System, the pre-Alpine terranes, composed of metamorphic sequences, are occasionally covered by Alpine metamorphosed Permo-Triassic sequences (Figure S1) [8, 16, 19–21]. It is important to note, however, that the highest Biharia Nappe System is

taken as a constituent of the Dacia megaunit according to a different interpretation as discussed elsewhere [8, 12, 13].

On the other hand, Hungary has a long history of exploration and production of HCs [22–24]. Among the principal producing areas, the southern part of the Pannonian Basin has an excellent HC potential. Several commercially important hydrocarbon occurrences are also known in the Szeged Basin, such as the Ásotthalom North (Ás-É), Dorozsma (Do), Kelebia North (Kel), Mórahalom (Móra), and the Szeged petroleum and natural gas fields (Figure 2). The most productive conventional HC reservoirs reside in the Neogene sediments (e.g., Miocene conglomerate and sandstone beds); nevertheless, important ones exist in the fractured crystalline (Kel and Do fields) and pre-Cenozoic volcanic (Kel field, fractured Permian rhyolite) and sedimentary (Móra and Szeged fields, brecciated Triassic dolomite) basement areas, about 1000–3000 m below the present surface [21–25]. Fortunately, during the crude oil exploration projects (from 1968 to 1985), several wells were drilled with intermittent usage of coring equipment in the Kelebia basement area (wells Kel and Ás-É). Some of them penetrated the basement top, which essentially consists of Variscan metamorphic rocks (e.g., gneiss and mica schist). Permian cover succession is also discovered locally [24].

The southern part of the basement of the Szeged Basin (Figures 1 and 2) contains blocks made up of medium-grade Variscan metamorphic rocks, Permian to Lower Triassic siliciclastic and volcanosedimentary formations (Korpád Sandstone, Jakabhegy Sandstone, and Gyűrűfű Rhyolite Formations, respectively), and shallow marine mudrocks and carbonates from the Middle Triassic (Szeged Dolomite Formation). Because of the tectonically induced uplift and erosion from the Late Cretaceous, the post-Triassic Mesozoic deposits are totally absent in the study area [16, 21, 24, 25]. The topographic undulations of the basement were covered by marine sediments during the Miocene (i.e., 20–10 Ma). Subsequently, the paleo-Danube and paleo-Tisza Rivers progressively filled the Pannonian Basin with clastic material, creating a thick Neogene non-marine succession [4, 7, 21–23].

The alluvial Korpád Sandstone Formation (Lower Permian) consists of red siliciclastic sedimentary rocks (dominated by sandstones and mudrocks) [16, 24]. Permian (263.4 ± 2.7 Ma, using the zircon U–Pb LA–SF–ICP–MS method) Gyűrűfű Rhyolite samples from the Kelebia area contain oriented, sericitized pumices, and broken subhedral (micro)phenocrysts (15–20 vol% quartz, 10–15 vol% altered plagioclase, and ~5 vol% altered biotite). Based on the primary composition and microtextural characteristics, these felsic volcanic rocks are rhyodacitic ignimbrites [26]. The Lower Triassic Jakabhegy Sandstone Formation, represented by gray, red, and lilac fluvial to shallow marine sandstones, covers the crystalline basement and older Permian rocks with unconformity [16, 21, 24]. The Late Anisian to Early Ladinian brecciated dark gray dolomite sequence, corresponding to the Szeged Dolomite Formation, shows evidence for multistage dolomitization [21].

2.2. Sampling. For mineralogical and petrographic analysis of the Permian terrigenous sedimentary and volcanogenic/

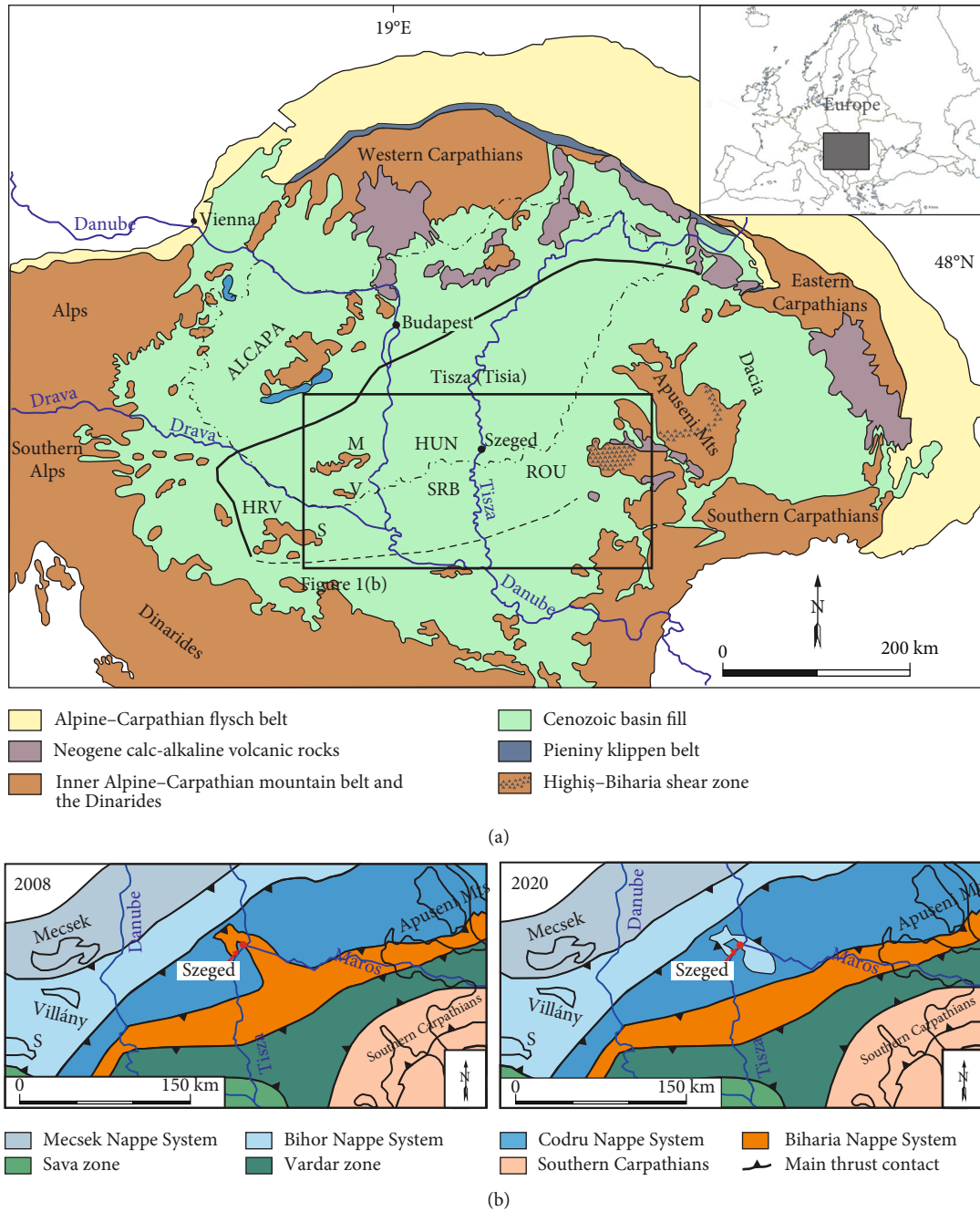


FIGURE 1: Geological framework. (a) The Alpine-Carpathian-Pannonian area [3, 14–16, 18]. Abbreviations: ALCAPA: Alpine-West Carpathian-Pannonian block; M: Mecsek Hills; S: Slavonian Mts; V: Villány Hills; HRV: Croatia; HUN: Hungary; ROU: Romania; and SRB: Serbia. (b) Main Alpine tectonic units of the study area according to a previous interpretation [12] and modified boundaries of the Alpine units based on a new concept [17]. Note that the fragments of the Biharia Nappe System have not been proven in Hungary based on the traditional Hungarian tectonic studies and maps [14–16]. Abbreviation: S: Slavonian Mts.

volcaniclastic rocks, the collections of archive thin sections at the host institution were studied from HC exploration wells near the village of Kelebia (Kel field; Permian red beds underlain by the ignimbrites, Permian ignimbrites, and volcaniclastic sedimentary rocks; Gyűrűfű Rhyolite Formation: wells Kelebia-7, 11, 12, 14, 22, and 23; Korpád Sandstone Formation: wells Kelebia-12 and 14) at depths of ~800–900 m below the surface (Figure 2). Additionally, corresponding to the scarcity of the basement cores, a total of 3

small core chips from the wells Kelebia-7 (877.5–879.5 m and 900.0–903.0 m; Gyűrűfű Rhyolite) and Kelebia-14 (905.0–910.0 m; Permian red beds underlain by the ignimbrites) were newly sampled for this study at the repository of the host institution (Table 1).

For Lower Triassic siliciclastic sedimentary rock characterization, core samples from the exploration well Mórahalom-1 (well Móra-1, Móra field) were examined (Figure 2). The available core section #17 (Jakabhegy Sandstone Formation) from

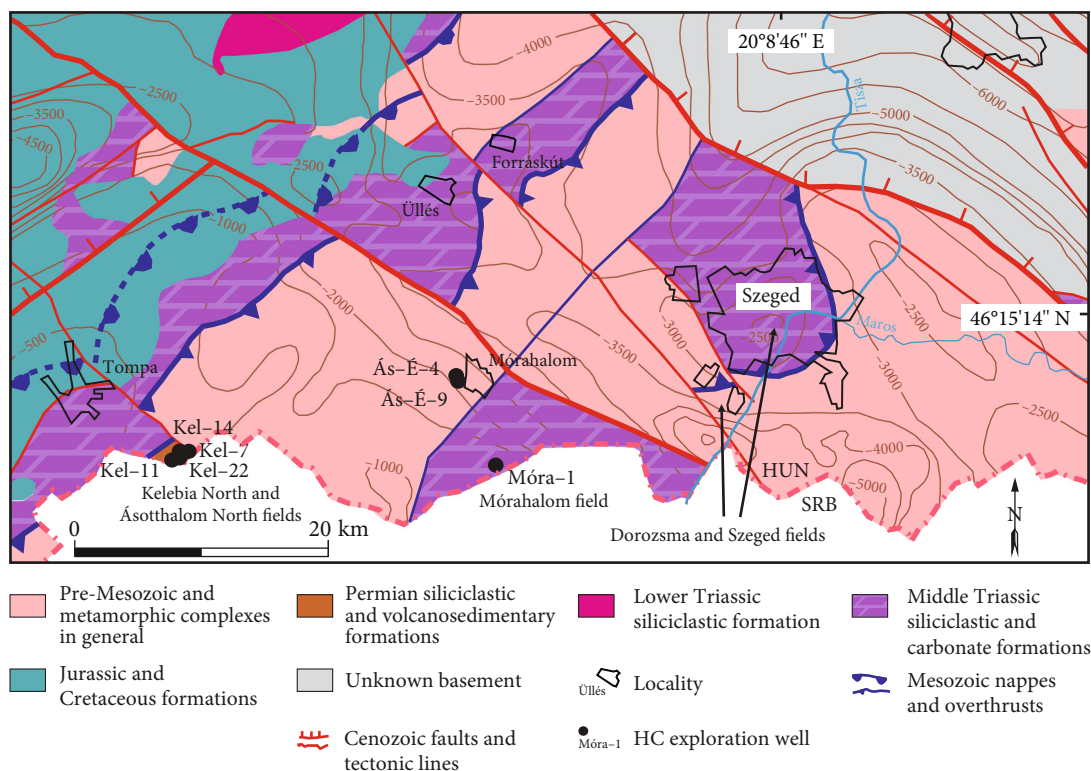


FIGURE 2: Location of the Kelebia basement area, together with other important HC fields in the Szeged Basin, on the generalized geological map of the pre-Cenozoic basement formations [14, 24]. Isoline numbers are in meters, showing basement depths and highs. Abbreviations: HUN: Hungary; SRB: Serbia.

the depth interval between 2306 and 2312 m below the surface was taken for detailed petrographic studies, including diagenetic and microtectonic observations. Additionally, the MOL Group (an integrated oil and gas company, Hungary) provided a covered thin-section collection from wells near the village of Ásotthalmom (Ás-É field) at depths of ~2000–2100 m below the surface. The available standard thin sections belong to the Lower Miocene marine conglomerate sequence, including reworked pebbles and cobbles of Jakabhegy Sandstones (Table 1).

2.3. Methodology of Mineralogical and Petrographic Analyses. Determination of the bulk mineralogical composition and characterization of the separated $<2\ \mu\text{m}$ grain size fraction of the selected Permian drill core chip samples ($n = 3$) was made by X-ray powder diffractometry (XRPD). The representative samples were measured by a Rigaku Ultima IV X-ray diffractometer using the Bragg-Brentano geometry (instrumental parameters: $\text{CuK}\alpha$ radiation, graphite monochromator, proportional counter, divergence, and detector slits of $2/3^\circ$). Macroscopically homogeneous rock chips were grounded and pulverized in an agate mortar. Random powder mounts were made using ~0.04 g rock powder on a Si single crystal sample holder to determine the bulk mineralogical composition. The qualitative and semiquantitative evaluation of the XRPD spectra was performed by the Rigaku PDXL 1.8 software (ICDD database,

PDF2010) and estimated based on the reference intensity ratio method, respectively.

Grain size separation for clay fraction ($<2\ \mu\text{m}$) analysis was achieved by repeated ultrasonic deflocculation and gravitational settling using Stokes' law. Highly oriented XRPD slides with $3\ \text{mg}/\text{cm}^2$ density were prepared by repeated sedimentation of the separated fraction on a standard glass sample holder. Both air-dried and ethylene glycol-solvated preparations were scanned at $45\ \text{kV}/35\ \text{mA}$, from 2 to $50^\circ 2\theta$ with goniometer step rate $1^\circ/\text{min}$ and step width 0.1° . Subsequently, the mounts were treated at 350 and 550°C and measured immediately after storage in a desiccator. Semiquantitative composition of the clay fraction was estimated following Moore and Reynolds' recommendation [27].

For the determination of illite "Crystallinity Index" and calculation of crystallite size, a triplicate scan of the same slide was run at $40\ \text{kV}/30\ \text{mA}$, from 3 to $14^\circ 2\theta$ with goniometer step rate $0.6^\circ/\text{min}$ and step width 0.01° . The determination of "crystallinity" was made using the Crystallinity Index Standards (CIS) of Warr and Rice [28] and the Kübler Index (KI_{Basel}) calculated after Warr and Mählmann [29] as discussed elsewhere [30]. Additionally, the illite crystallite size was determined by a routine single peak method (on the 001 reflection of the K-white mica) using the Scherrer equation embedded in the PDXL 1.8 software. For differentiation between K-, Na-, and Ca-rich white micas (i.e., illite, paragonite, and margarite), the XRPD (00,10) basal reflections

TABLE 1: Sample descriptions.

Location	Formation	Borehole (core number)	Sample code	Depth (m)	Type
Kel field	Permian red beds (underlain by the ignimbrites)	Kel-14 (#3)	ÁGK-244, no. 153	905.0	Thin sections and core chip
	Gyűrűfű Rhyolite (Permian ignimbrites)	Kel-7 (#6)	ÁGK-230, no. 24	869.5 and 870.2	Thin sections
		Kel-7 (#7)	ÁGK-231, no. 142	877.5	Thin sections and core chip
		Kel-7 (#8)	ÁGK-232	900.0	Thin section and core chip
		Kel-11 (#5)	ÁGK-240, no. 150	863.0	Thin sections
		Kel-12 (#1)	ÁGK-242, no. 151	836.0	Thin section
		Kel-14 (#4)	ÁGK-245	928.0	—
		Kel-22 (#10)	ÁGK-251, no. 158	823.0	Thin section
		Kel-22 (#12)	ÁGK-252	828.0	Thin section
		Kel-22 (#18)	ÁGK-253, no. 160	843.0	Thin section
		Kel-22 (#23)	ÁGK-254, no. 161	860.5	Thin sections
		Kel-23 (#3)	ÁGK-1866	833.0	Thin section
		Korpád Sandstone (overlain by the ignimbrites)	Kel-12 (#3)	ÁGK-243, no. 152	871.5
Ás-É field	Lower Miocene conglomerate (Triassic pebbles)	Ás-É-4 (#3)		1,963	Thin sections
		Ás-É-9 (#2)		2,045	Thin sections
Móra field	Jakabhegy Sandstone (Lower Triassic)	Móra-1 (#17)	M-1/17/1A, M-1/17/2	2,306	Thin sections and core chip

around 2 Å were checked using highly oriented slides as discussed elsewhere [31, 32]. For a better resolution and precise determination of the position of the 00,10 K-white mica peaks, triplicate analyses were performed at 50 kV/40 mA, from 40 to 50°2 θ with a goniometer scan speed of 0.5°/min and a step width of 0.02°.

Petrographic studies were conducted on small hand specimens ($n = 8$) and standard thin sections ($n = 30$) that were studied by polarized light microscopy using an Olympus BX41 microscope. Framework grains of sandstones were classified by common micropetrographic methods [33, 34]. The microstructural analysis of the samples is based on Passchier and Trouw [35]. However, notice that there is no information on the definite orientation of the core samples studied. Cathodoluminescence (CL) microscopy of selected Gyűrűfű samples was carried out using a Reliotron VII type cold CL device operating at a 7 kV accelerating voltage and 0.7 mA beam current, mounted on an Olympus BX43 microscope. Photomicrographs were made using an Olympus DP73 digital microscope camera. Conventional mineral abbreviations have been used during the whole paper [36].

3. Results and Discussion

3.1. XRPD Data: Mineralogical Composition and Characteristics of the <2 μ m Fraction. Based on semiquantitative XRPD analyses, the bulk volcanoclastic samples (Gyűrűfű Rhyolite) have a rather uniform composition (expressed

in mass%). Quartz (40–50%) and white mica (illite±muscovite, 30–50%) are the major components with some K-feldspar (~5%) and trace amount of plagioclase (albite), chlorite, dolomite, and hematite. As far as the red bed sample studied is concerned, it has a bulk composition of high amounts of white mica (70–80%) and quartz (20–30%). Some chlorite, plagioclase, and hematite were also detected, but K-feldspar and dolomite phases are missing relative to the bulk volcanoclastic samples (Figure 3(a)).

The mineralogical composition of the <2 μ m fraction of both studied lithologies is rather similar: white mica is the predominant phase (>90%) with minor chlorite and a trace amount of quartz±hematite (Figure 3(b)). Regarding the clay fraction of the red bed sample, the position of the peak 00,10 shows a 1.9927 ± 0.0001 Åd spacing (Figure 4). This value together with the lack of shoulders on any side of this reflection suggests a near-theoretical “muscovite” (K-white mica) mineralogical composition without any Ca or Na substitutions [37]. After the saturation of the samples with ethylene glycol, the XRPD patterns prove that the K-white mica does not contain a detectable swelling phase (i.e., smectitic interstratification). The Esquevin index value [38] is ~0.26 which indicates a significant Fe substitution and, consequently, phengitic composition for the K-white mica of the studied red bed sample. The determined KI_{Basel} value refers 0.244 ± 0.007 (Figure 5(a)), close to the anchizone–epizone boundary ($KI = 0.25$) [39–42]. The main apparent crystallite size of K-white mica corresponds to $\sim 600 \pm 30$ Å which is

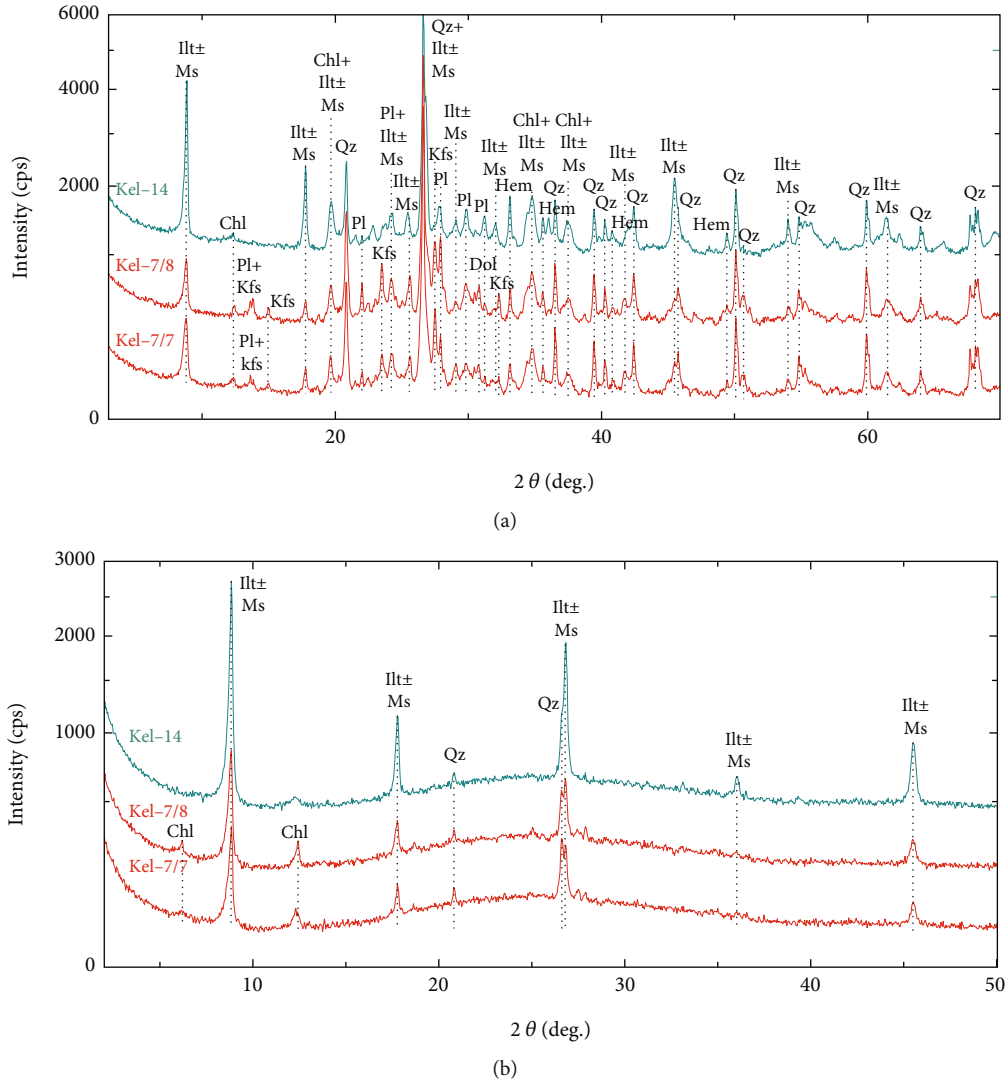


FIGURE 3: X-ray powder diffractograms of the studied samples (sample Kel-14: Permian red beds; samples Kel-7/7 and 7/8: Gyűrűfü ignimbrites; for further information, see Table 1). (a) XRPD pattern of the bulk rock samples; (b) XRPD pattern of the separated clay fraction samples (air-dry). Abbreviations: Chl: chlorite; Dol: dolomite; Hem: hematite; Illt±Ms: illite±muscovite; Kfs: K-feldspar; Pl: plagioclase; Qz: quartz.

close to the anchizone–epizone transition (~ 520 Å) [43]. Consequently, XRPD data suggest a very low- to low-grade metamorphism of the Permian sequence at $\sim 300^\circ\text{C}$ peak metamorphic temperature (Figure 5(b)).

3.2. Petrographic Fingerprints of Low-Grade Metamorphic Processes

3.2.1. Permian Siliciclastic Rocks. The fine-grained matrix of the Korpád samples overlain by ignimbrites has a weakly to moderately developed foliation with oriented sericite-rich (white mica) bands. Broken crystals of volcanic quartz, plagioclase, and muscovite occur as silt- to sand-sized detrital grains (Figures 6(a)–6(d)). Occasionally, tiny rhombohedral carbonate crystals with a somewhat saddle-like shape (likely dolomite, first generation) appear in the matrix. In the overlying Gyűrűfü ignimbrites, the

presence of dolomite was confirmed using the XRPD method (Figure 3(a)). The larger grains of dolomite (~ 200 – $400\ \mu\text{m}$) are strongly undulatory, show curved crystal boundaries, and have fibrous strain shadows subparallel to the foliation (Figures 6(c) and 6(d)). Around the core objects, displacement-controlled carbonate (dolomite, second generation)+hematite fringes were first developed, following quartz fringes. In a ductile deforming rock, such strain shadows were commonly formed by precipitation from the solution in the case of low-T deformation and high fluid pressure [35].

The studied red bed samples, overlying the Gyűrűfü ignimbrites, are composed of relatively well-foliated pale green to red fine-grained rocks, showing a slaty appearance. On the thin-section scale, spaced cleavage is defined by fine-grained micaceous material with detrital quartz and muscovite stacks in microlithons (Figures 6(e) and 6(f)).

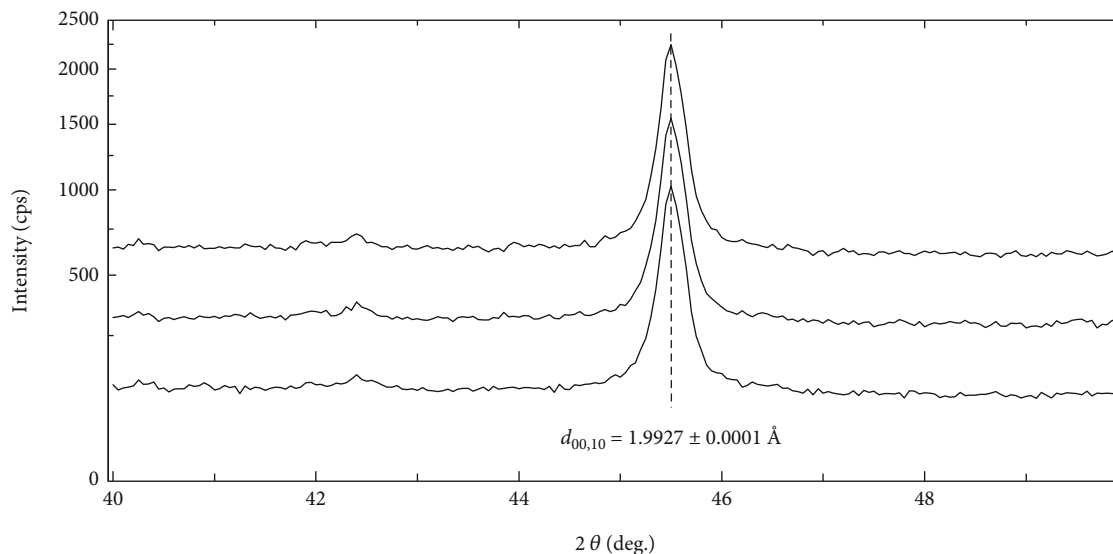


FIGURE 4: XRPD patterns of (00,10) basal reflection of the studied red bed sample measured in triplicate (sample Kel-14; $<2\ \mu\text{m}$ fraction, air-dry, highly oriented specimen). The d spacing of $1.9927 \pm 0.0001\ \text{\AA}$ indicates near pure “muscovite” composition of the white mica.

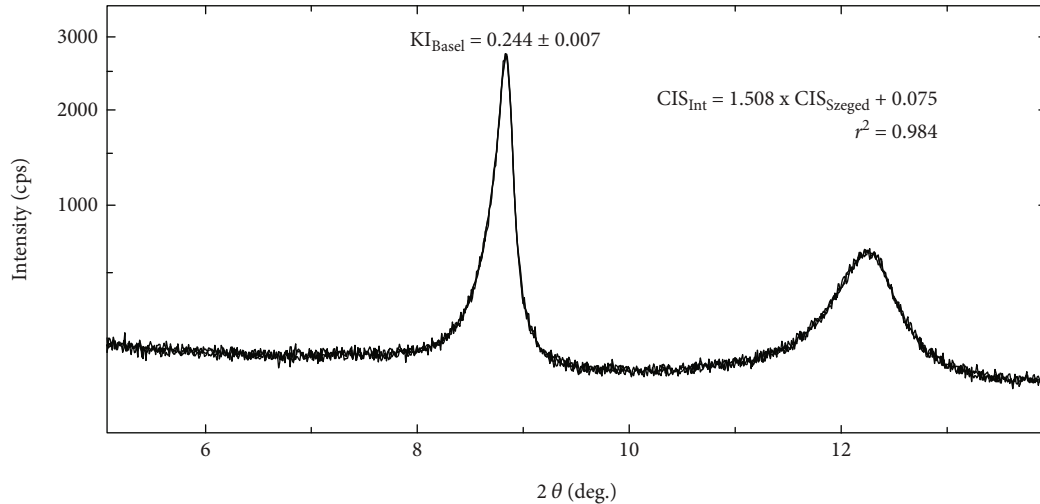
3.2.2. Permian Ignimbrites. In the Kelebia area, the samples of the Gyúrúfű Rhyolite Formation contain ca. 30–50 vol% crystal fragments with an assemblage of quartz+K-feldspar +plagioclase+biotite and ca. 5–10% altered pumice clasts (sericitized) that float in a devitrified and strongly recrystallized groundmass. Moreover, there are some accessory minerals such as apatite, zircon, and opaque grains. Feldspars are partially replaced by dolomite and/or reflect features of sericitic alteration. Mafic minerals (biotite, rare pyroxene) are also moderately to strongly altered (Figure 7).

On the thin-section scale, several deformation features were recognized in the studied ignimbrite samples, showing a weakly to moderately developed disjunctive foliation (in the sense of Passchier and Trouw [35]). Quartz phenocrysts are frequently fractured, fragmented, and variably deformed, so evidence of the original crystal shape is generally absent. Crystal fragments are typically angular in shape; however, the resorbed crystal outlines are rarely recognizable. Broken quartz crystal fragments also show some evidence of rotation and displacement. Quartz grains mostly show undulatory extinction and deformation lamellae in cross-polarized light and exhibit a low-intensity blue (core region) to relatively high-intensity violet-red (rim) reverse zoning luminescence pattern in CL (Figure 7 and Figure S2). Furthermore, domino-type and mosaic fragmented quartz clasts (porphyroclasts in the sense of Passchier and Trouw [35] as discussed below) are common (Figure 8 and Figure S2).

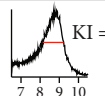
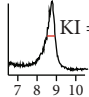
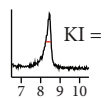
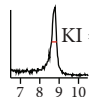
Understanding the origin of broken and fragmented crystals in volcanic deposits can often be challenging, as many crystal-rich ignimbrites contain extensively fragmented crystals [35, 44]. According to van Zalinge et al. [44], primary fragmentation caused by rapid decompression is associated with the eruption, whereas secondary fragmentation is related to compaction and welding. Generally, the primary process is characterized by an extensive crystal breakage and expansion

of individual crystals (~5 vol%), but their original shapes are preserved. The secondary one is generally associated with enhanced fragmentation localized at points of contact between adjacent fragments, resulting in loss of volume between them [44]. Secondary fragmentation increases the crystal aspect ratio, therefore forming textures that resemble mantled porphyroclasts (i.e., crystals with a rim, which is of the same composition as the clast) in shear zones [35, 44–46]. Based on our micropetrographic observations (e.g., presence of deformation lamellae, domino-type and mosaic fragmented crystals with rotated chips, absence of welded pumice clasts, and insignificant amounts of mantled clasts), we suggest that the above-mentioned features of brittle fracturing together with the ductile (intracrystalline) deformation of quartz (Figure 8 and Figure S2) reflect signs of tectonic processes (e.g., pure to simple shear) in a variously deformed ignimbrite, instead of compaction and welding.

In the moderately well-foliated samples (e.g., well Kel-7 cores #7 and #8, well Kel-12 core #1, and well Kel-23 core #3), the cleavage domains are rich in white mica (i.e., sericite and/or muscovite) subparallel to the trend of the domains. In microlithons, fibrous or elongated strain shadows are common on both sides of the core object (e.g., white mica strain fringe around apatite and quartz strain shadow around dolomite, respectively). Such strain shadows are composed of white mica around the quartz porphyroclasts, showing a gradual transition between the fringes and the recrystallized matrix (Figure 8 and Figure S2). Mantled quartz clasts also occur locally (sample Kel-23). It is important to note that mechanical twins can be distinguished in replacement dolomite (first generation). Additionally, between the quartz porphyroclast fragments, some undeformed dolomite rhombs (second generation) appear in the recrystallized matrix (Figure 8), reflecting postkinematic mineralizing fluids.



(a)

Metapelitic zone (depth) (km)	Temperature (°C)	Characteristic pelitic rock type	Metamorphic facies	Illite crystallinity (IC): Kübler Index, KI ($\Delta^2\theta$) with characteristic XRPD-plots of the 10 Å-peak of illite
Early diagenetic zone 3.5–4	~100	Shale/ mudstone	Zeolite	~1.00  Low grade diagenesis
Late diagenetic zone 6.5–8				0.42  Limit of diagenesis - anchizone
Low anchizone	~200	Slate	Prehnite–pumpellyite	0.30  Anchizone
High anchizone 10–12				0.25  Limit of anchizone - epizone
epizone				

(b)

FIGURE 5: Determination of illite “Crystallinity Index” (IC). (a) XRPD patterns of (001) basal reflection of the studied red bed (slate) sample measured in triplicate (sample Kel-14; $<2\mu\text{m}$ fraction, air-dry, highly oriented specimen) used for IC determination. Equation for conversion of own data to KI_{Basel} [39] is also indicated; (b) metapelitic zones showing associated rock types and metamorphic facies. Notice that the correlation with the Kübler Index [39–42] is also shown.

3.2.3. Triassic Siliciclastic Rocks. The Triassic sandstone samples from the Móra field are moderately to well-sorted subarkose to quartz arenite ($>95\%$ quartz). They are pink or pale red through hematite pigmentation; additionally, fossils are absent. The samples are composed of rounded mono- and polycrystalline quartz and lesser amounts of K-feldspar (microcline) and volcanic grains. Accessories are zircon and tourmaline. Quartz cement as syntaxial overgrowths is common. Deformation lamellae occur in both the original quartz framework grain and its overgrowth. Microcrystalline silica and carbonate replacements are also typical. Locally, wide ($>1\mu\text{m}$) deformation twins were developed in the replacement carbonate crystals. Additionally, the occurrence of tiny quartz veinlets and transgranular microcracks marked by fluid inclusion planes (FIPs) is a characteristic feature of the

samples (Figure 9 and Figure S3). These signs reflect that fluids have to be involved in the cementation of brittle dilatational microfaults.

In the Ásotthalom area, belonging to the Ás–É field, the Lower Miocene conglomerate samples are composed of acidic volcanic, metamorphic (quartz-sericite/muscovite schist), and sedimentary rock clasts derived from the pre-Neogene basement (Figure S4). Quartzite and quartz arenite clasts are the main components, showing strong similarities with the Triassic sandstones in the study area (Figure 10). The appearance of deformation lamellae in quartz overgrowth cement together with quartz veinlets and FIPs in quartz arenite clasts clearly indicates that the time of ductile and brittle deformation and contemporaneous fluid migration preceded the Neogene uplift and erosion (i.e., partial subaqueous exposure).

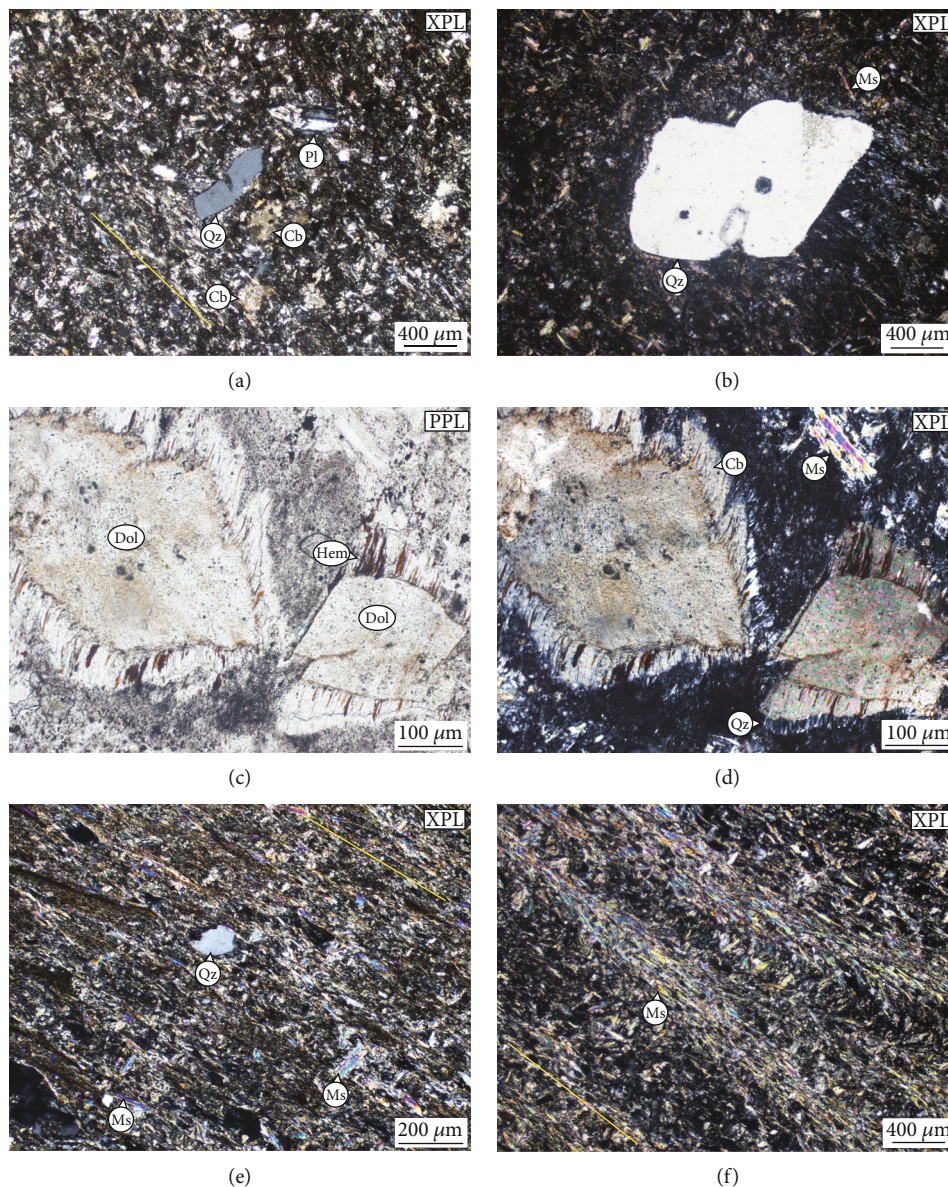


FIGURE 6: Thin-section photomicrographs of the Permian siliciclastic rocks ((a–d) well Kel-12 core #3; (e, f) well Kel-14 core #3). (a) Broken quartz and plagioclase crystals in the fine-grained matrix showing a weakly developed foliation (yellow line). Note: selective carbonatization of the matrix material. (b) A broken resorbed crystal of volcanic quartz. (c, d) Strain fringes around saddle dolomite core objects which show sweeping extinction. (e, f) Domainal spaced cleavage (foliation is indicated by the yellow line) with quartz and muscovite stacks in microlithons. Abbreviations: PPL: plane-polarized light; XPL: cross-polarized light; Cb: carbonate; Dol: dolomite; Hem: hematite; Ms: muscovite (detrital); Pl: plagioclase; Qz: quartz.

3.3. *Diagenesis versus Metamorphism: Evaluation of the Temperature Conditions.* To establish the T (and P) conditions reached by the studied rocks of the Permo-Triassic noncarbonate cover succession in the Kelebia basement area, mainly temperature-dependent characteristics are evaluated and interpreted (Table 2). The slaty appearance, together with the disjunctive foliation, is one of the most striking features of the Permian samples subjected to increased T and P, corresponding to very low- to low-grade metamorphic conditions at temperatures greater than 200–250°C [35, 46–48]. Based on the XRPD data (KI_{Basel} value and the main apparent crystallite size of the K-white mica), corresponding to a

progressive trend of phyllosilicate crystal chemical changes [39–43, 47, 48], a peak metamorphic temperature of ~300°C (anchizone–epizone boundary) can be proposed.

Additionally, deformation lamellae in tectonically deformed quartz and twin morphology in carbonate minerals, especially in calcite, can be used as a crude geothermometer [35, 45, 46, 49]. The plasticity of quartz is generally restricted to temperatures greater than 200°C, and the presence of deformation lamellae could be taken as a qualitative indicator of relatively high stress levels. At low-grade conditions (300–400°C) undulose extinction of quartz and deformation lamellae in a subparallel, nonplanar arrangements

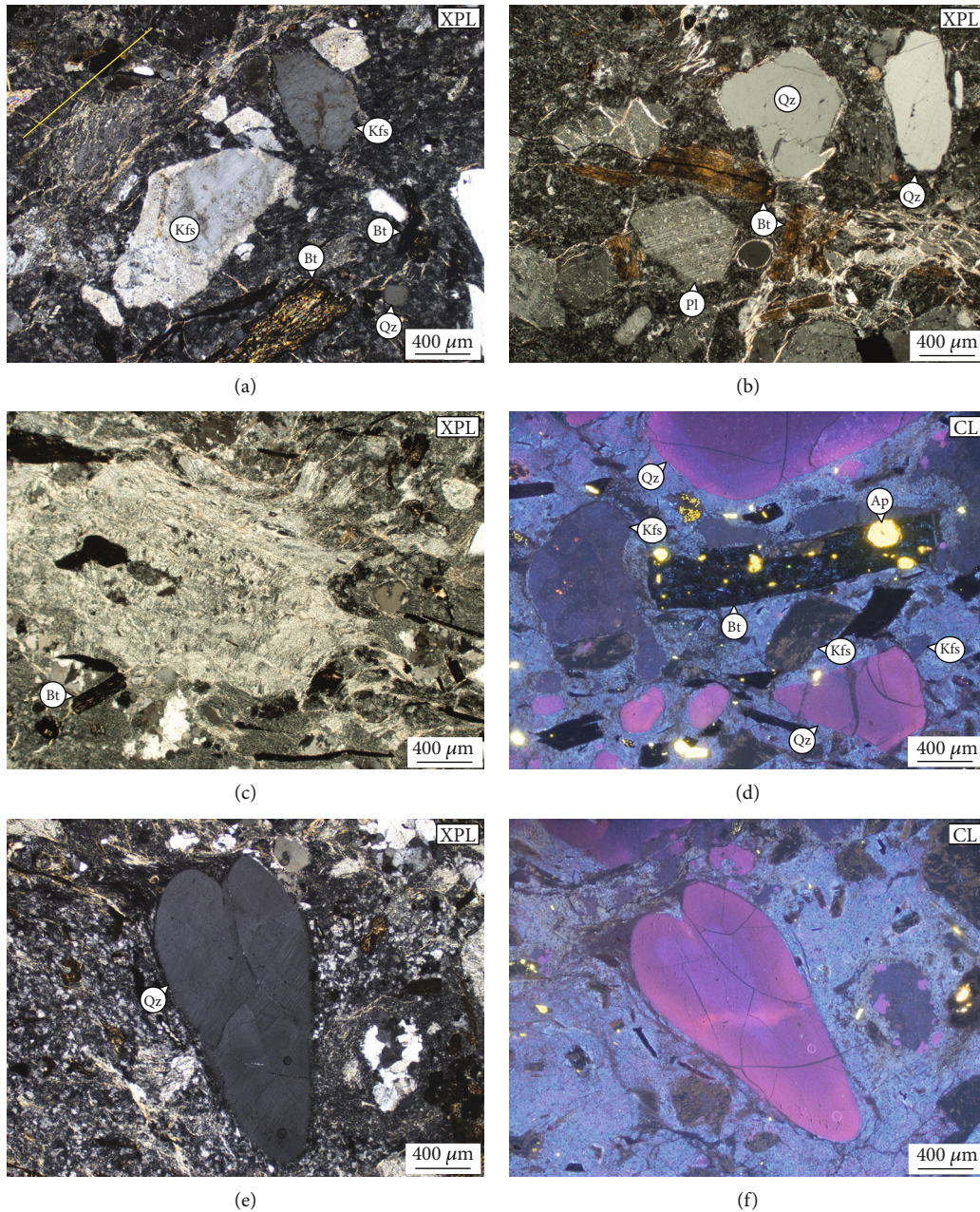


FIGURE 7: Thin-section photomicrographs of the Permian ignimbrites: crystal and juvenile components ((a, c–f) well Kel-7 core #8; (b) well Kel-11 core #5). (a, b) Crystal fragments in the fine-grained matrix showing a weakly developed foliation (yellow line in a). Note: the strongly altered (flattened and sericitized) pumice shards are oriented, and the feldspar also reflects sericitic alterations. (c) Altered juvenile components (sericitized pumice and pumice shards). In the relict pumice clast, the original internal vesicular microstructure has been destroyed. (d) Fractured quartz, altered broken K-feldspar, and apatite+opaque mineral pseudomorphs after biotite in the strongly recrystallized groundmass. Quartz crystals and fragments generally exhibit a reverse zoning pattern with low-intensity blue CL cores overgrown by a relatively high-intensity red CL rim. Small apatite grains show uniform bright yellow luminescence. (e, f) A resorbed and deformed crystal of volcanic quartz displaying variable blue to red (rim and embayments) CL colors. Abbreviations: PPL: plane-polarized light; XPL: cross-polarized light; CL: cathodoluminescence; Ap: apatite; Bt: biotite; Kfs: K-feldspar; Pl: plagioclase; Qz: quartz.

are characteristic structures [35, 46, 49, 50]. On the other hand, plasticity in the form of twinning can appear even at room temperature in calcite (type I). Wider twins that can be optically resolved (type II $> 1 \mu\text{m}$) dominate above 200°C up to 300°C ; however, twinning apparently does not develop below 300°C in dolomite [35, 45, 49]. Mechanical

twinning in dolomite requires higher critical resolved shear stress, and so it is activated at higher T compared to calcite [45]. All of these observations coincide with the high anchi-zone–epizone values mentioned above.

Another important property of quartz is the variability of its CL characteristics in dependence on the specific origin

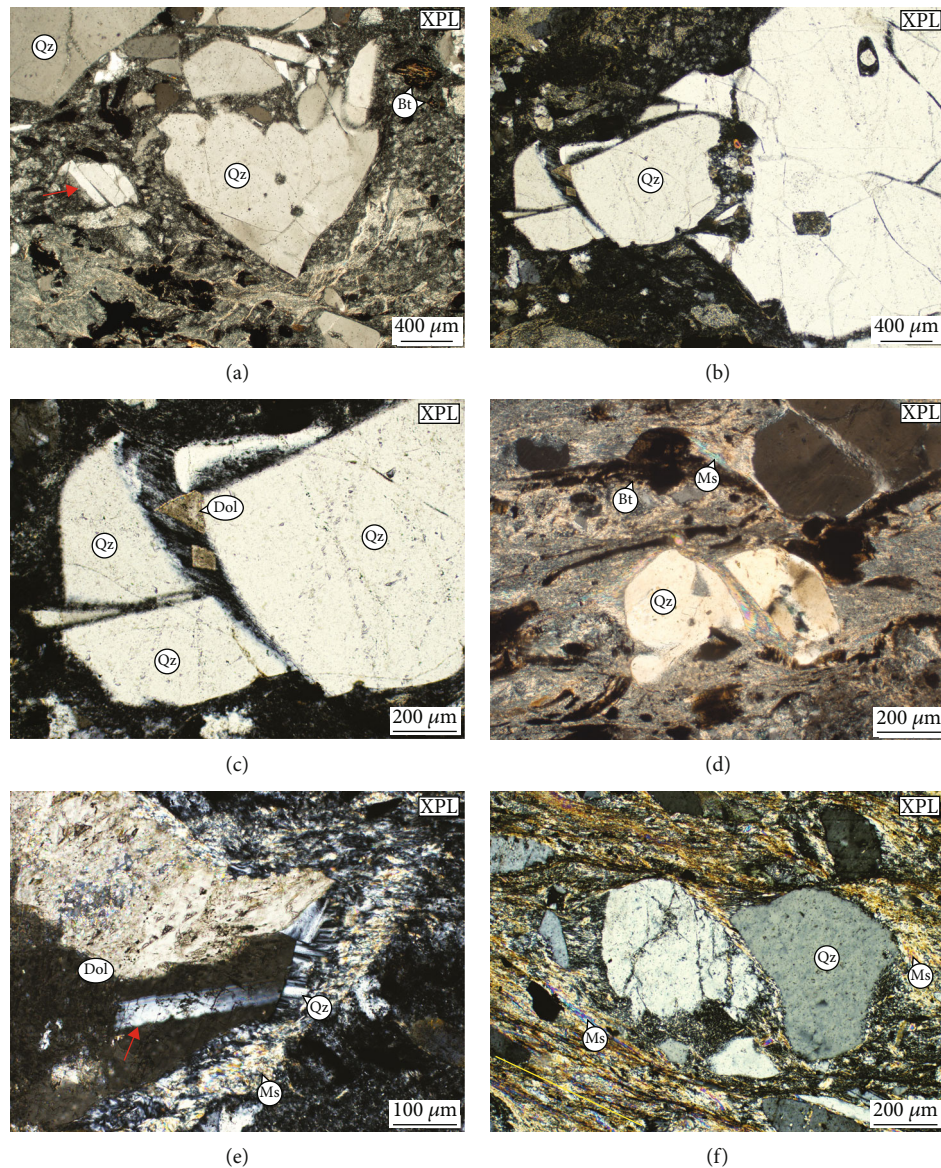


FIGURE 8: Thin-section photomicrographs of the Permian ignimbrites: deformation textures ((a–c, e) well Kel-7 core #8; (d) well Kel-7 core #7; (f) well Kel-23 core #3). (a) Domino-type fragmented quartz porphyroclast (red arrow). (b, c) Mosaic fragmented quartz porphyroclast. Note: fragmentation is postdated by dolomite crystallization in the matrix. (d) White mica strain shadows around fragmented quartz porphyroclasts in a finer grained matrix (the section is normal to the foliation). (e) Elongated quartz strain shadow around a dolomite replacing an earlier feldspar phenocryst. Note: mechanical twinning in dolomite (red arrow). (f) Disjunctive foliation in a deformed ignimbrite sample (the trend of the cleavage domains is indicated by the yellow line; the section is normal to the foliation). Note: strain shadows are associated with strain caps. Abbreviations: XPL: cross-polarized light; Bt: biotite; Dol: dolomite; Ms: muscovite; Qz: quartz; Zrn: zircon.

(e.g., different grades of metamorphism) [51, 52]. A typical brown CL of quartz is a characteristic feature of low-T metamorphic rocks, whereas quartz derived from metamorphic conditions with temperatures above 500°C exclusively exhibits visible blue CL that is possibly related to recrystallization processes [52]. The CL study of the Permian ignimbrites from the Kelebia area indicated that homogenous blue CL was not observed, so such high-T conditions can be excluded. Quartz crystals with low-intensity blue CL cores overgrown by a relatively high-intensity violet-red CL rim (reverse zoning; Figure 7) can exhibit the original mag-

matic features. According to Vernon [46], blue to violet CL colors are associated with enrichment in Ti. Based on evidence from quartz compositional zoning and titanium-in-quartz geothermometry, bright-CL rims are generally Ti-richer than dark-CL cores in ignimbrite units, reflecting a magmatic recharge event as a potential eruption trigger [53, 54]. This phenomenon is consistent with the genetic interpretation of the Gyűrűfü Rhyolite Formation in the study area [26].

It is noteworthy that the determination of metamorphic conditions in very low- to low-grade metamorphic

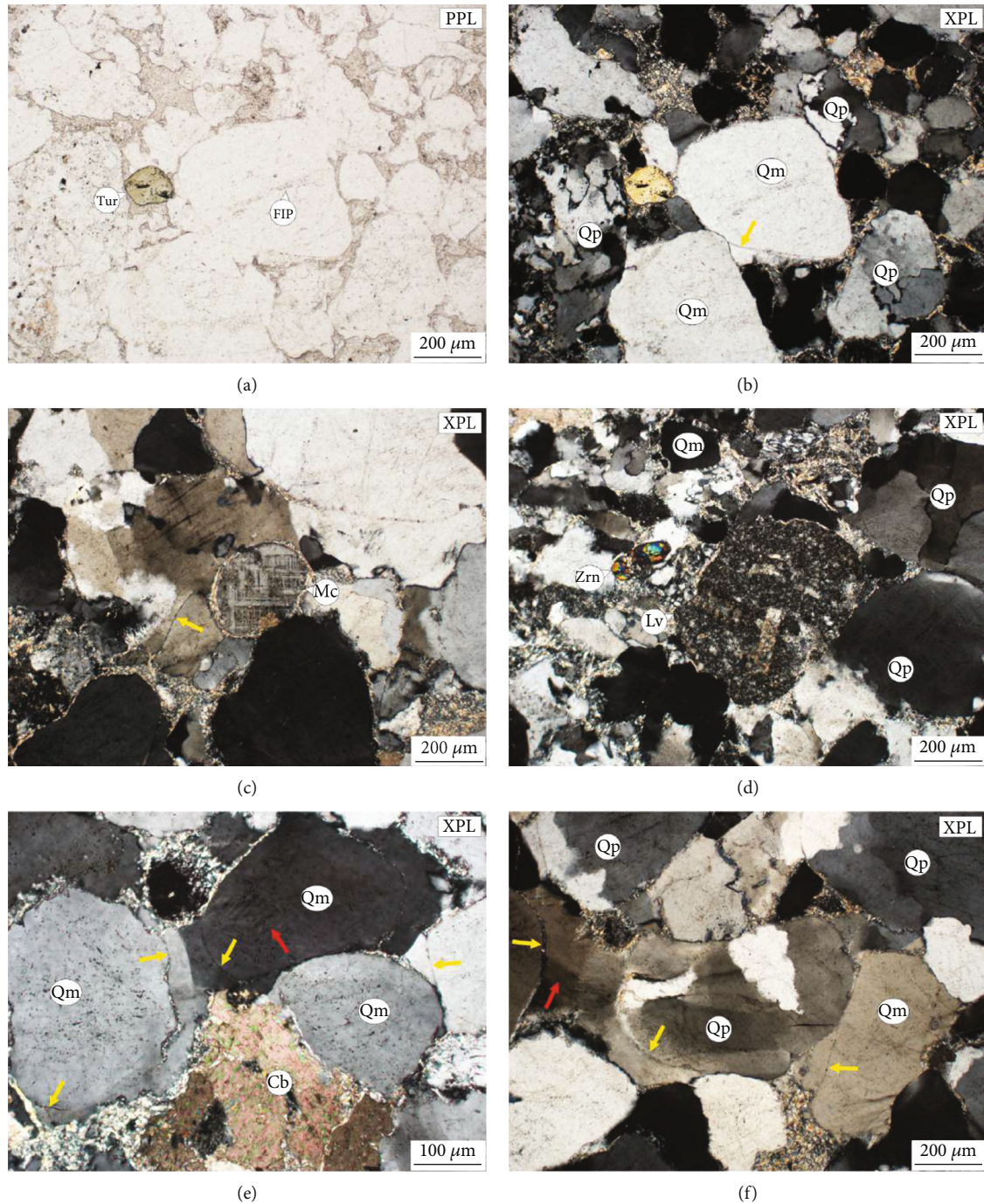


FIGURE 9: Thin-section photomicrographs of Lower Triassic sandstones showing a mature composition of quartz arenite (well Móra-1 core #17). (a–d) Rounded framework grains and accessory minerals. Notice the line of inclusions marked by yellow arrows showing the original grain boundary. Quartz grains and overgrowths are frequently replaced by microcrystalline silica. Sets of parallel microcracks marked by fluid inclusion plains also occur. (e, f) Overgrowth cement is postdated by silica and carbonate replacement. The original grain boundaries are visible as lines of tiny inclusions (yellow arrows). Note: deformation lamellae in quartz (red arrow). Abbreviations: PPL: plane-polarized light; XPL: cross-polarized light; FIP: fluid inclusion plain; Cb: carbonate; Lv: volcanic lithic fragment; Mc: microcline; Tur: tourmaline; Qm: monocrystalline quartz; Qp: polycrystalline quartz; Zrn: zircon.

successions of (silici)clastic rocks is not an easy task [42, 48]. However, specific criteria, such as crystallite size values and crystal chemical parameters of the sheet silicates or other temperature-dependent petrographic characteristics summarized in Table 2, can be considered as evidence for the

progressive metamorphism of the studied units. Taking notice of the different positions in the geological literature on the existence or absence of prograde metamorphic post-Variscan cover formations within the Codru Nappe System [8, 16, 20, 26, 55], the mineralogical and petrological data

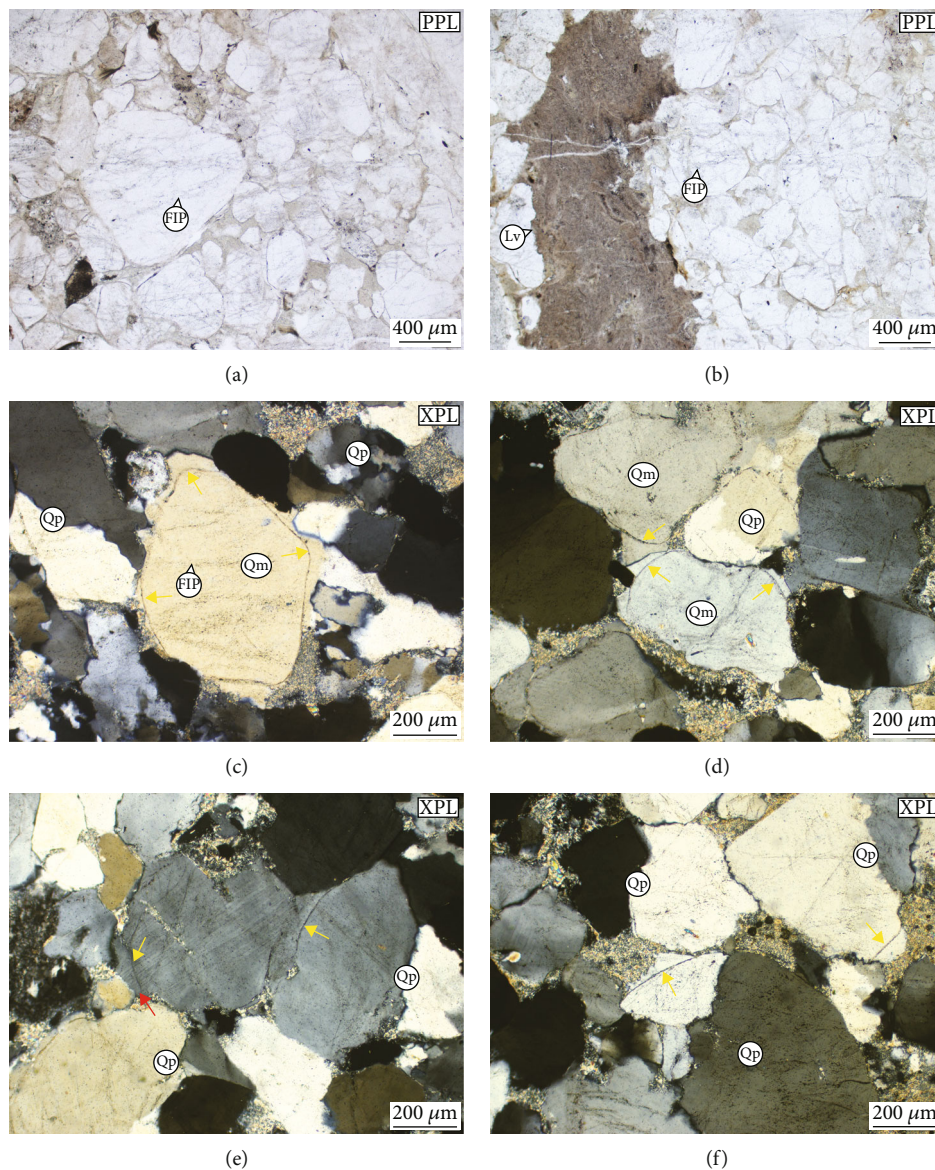


FIGURE 10: Thin-section photomicrographs of the Triassic sandstone clasts separated from the Lower Miocene conglomerate ((a–d, f) well *Ás-É-4* core #3; (e) well *Ás-É-9* core #2). (a, b) Sets of parallel transgranular microcracks marked by fluid inclusion plains together with tiny quartz veinlets (see volcanic lithic grain). (c–f) Rounded framework grains with syntaxial quartz overgrowths. Notice that the yellow arrows show the original grain boundary. Marginal parts of the detrital quartz grains and/or overgrowth cement are partially replaced by microcrystalline silica. Note: deformation lamellae in both the original quartz grain and its overgrowth (red arrow), reflecting that the lamellae developed after cementation. Abbreviations: PPL: plane-polarized light; XPL: cross-polarized light; FIP: fluid inclusion plain; Lv: volcanic lithic fragment; Qm: monocrystalline quartz; Qp: polycrystalline quartz.

presented here clearly reflect that the Permo-Triassic non-carbonate cover succession in the Kelebia basement area suffered a high anchizonal to epizonal (~greenschist facies) metamorphic alteration after their deposition.

The abovementioned results are consistent with the lithological interpretation of wells in northern Vojvodina and in the southern part of the Neogene Pannonian Basin, Serbia, close to the study area. The wells at Palić (~27 km SE of Kelebia) penetrated a low-grade Permian metamorphic sequence composed of schistose, reddish brown to grayish green metasiltstones and metasandstones, alternating with rhyolitic to rhyodacitic volcanic and volcanoclastic rocks [56].

3.4. Time–Temperature Path of the Kelebia Basement Area: Tectonothermal Evolution. Based on detailed petrographic investigations and interpretation, a tentative time–temperature (depth, qualitative) path is summarized in Figure 11. Clearly, the observed Permian and Triassic rocks were deposited in continental environments. Based on well-rounded grains, good sorting, and high textural maturity together with a compositional maturity (i.e., quartz arenites), the studied Triassic sandstone samples, at least partially, are interpreted to be of aeolian origin [34]. A published burial model for Korpád and Jakabhegy Sandstones is not available; however, we suggest that the initial subsidence during the

TABLE 2: Temperature-dependent structural and textural features of the studied rock samples.

Rock type	Mineralogical and/or petrographic features	Characteristic temperature (°C)
Permian siliciclastic rocks	$KI_{\text{Basel}} = 0.244 \pm 0.007$; crystallite size (K – white mica) = $600 \pm 30 \text{ \AA}$	~300
	Slaty appearance, domain spaced cleavage, and fibrous strain shadows subparallel to the foliation	>200–250
Permian ignimbrites	Disjunctive foliation and strain shadows	>200–250
	Undulatory extinction and deformation lamellae in quartz	>200, generally 300–400
	Mechanical twins in replacement dolomite	> 300
	Inherited blue to red CL colors of quartz	<500
Lower Triassic siliciclastic rocks	Deformation lamellae in both the original quartz grain and its overgrowth	>200, generally 300–400
	Thick (type II > 1 μm) twins in replacement carbonate	>200, generally 200–300 (valid and calibrated in the case of calcite)

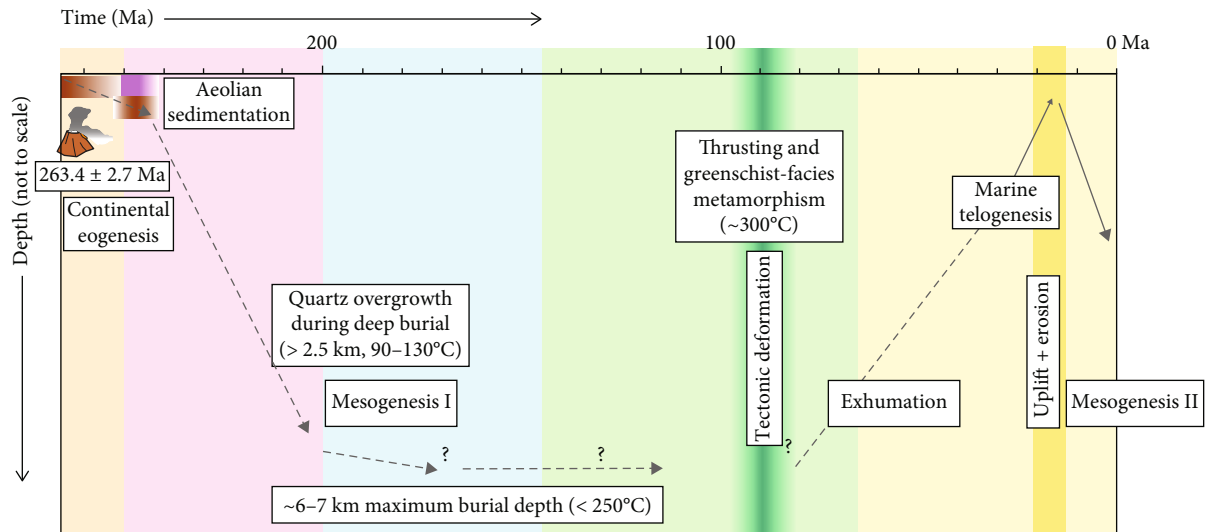


FIGURE 11: Tentative time–temperature path of the Kelebia basement area. According to Worden and Burley [57], three conceptual regimes of diagenesis are indicated: (i) eogenesis (early diagenesis), (ii) mesogenesis (burial diagenesis), and (iii) telogenesis (uplift-related diagenesis).

Middle to Late Triassic was relatively rapid (mesogenesis I). The formation of replacive saddle dolomite (Figure 6) is generally a late diagenetic event and requires minimum temperatures of 60 to 80°C (typically 90 to 160°C) [21, 58]. Additionally, the precipitation of syntaxial quartz overgrowths in most sedimentary basins occurs during deep burial (>2.5 km) diagenesis at elevated temperatures (typically 90 to 130°C) [59]. In the study area, Lower Triassic sandstones are overlain by marine sequences, including Middle Triassic nonmetamorphic carbonates (Szeged Dolomite Formation) with a maximum burial depth of approximately 5–6 km (<200°C, corresponding to a normal geothermal gradient of 35°C/km) before the Late Cretaceous to Paleogene inversion and exhumation [21]. Therefore, the maximum burial depth for the oldest studied units (Permian siliciclastics and ignimbrites) is proposed to be at 6–7 km (Figure 11). The burial model proposed for the Upper Perm-

ian deposits (Mecsek Hills, southern Hungary, ~160 km W of Kelebia; Figure 1(a)) agrees with a burial that reaches 200–250°C in the Early Jurassic [60].

On the other hand, the appearance of the deformational microstructures (e.g., disjunctive foliation, tectonically deformed quartz, and twin morphology of carbonate minerals; Figures 8 and 10) unequivocally indicates that the Permo-Triassic sequence was subject to tectonic stress before the Early Miocene uplift and erosion which later stage corresponds to an exhumed position close to the coeval surface (Figure 11). Within the ACD system, undoubtedly, the most significant orogenic events are related to the thrusting and nappe stacking during the Cretaceous [4–12]. Very likely, these tectonic processes favored the prograde reaction series of phyllosilicates (~300°C temperature for the peak metamorphism), instead of burial depth.

Unfortunately, the Alpine orogenic phases that shaped the pre-Neogene basement in the Kelebia basement area are poorly studied in terms of kinematics and timing of deformation. Nevertheless, five tectonic events were proved in the nearby Apuseni Mountains (Figure 1(a)): (i) Late Jurassic obduction of the Transylvanian ophiolites (D0), (ii) late Early Cretaceous (~130 Ma) nappe stacking (D1, “Austrian” phase), (iii) Early–Late Cretaceous (110–90 Ma) nappe stacking (D2, “Intra-Turonian” or “Turonian” phase), (iv) Late Cretaceous extension and differential exhumation (D3), and (v) latest Late Cretaceous–Early Paleogene compression with brittle conditions (D4, “Laramian” phase) [6, 8]. It is important to note that no evidence of the D0 and D1 phases can be found in the Tisza megaunit [6, 8, 17]. During the D1 phase, the Biharia Nappe System, being a part of the Dacia megaunit [12, 13], was buried to a minimum of 8 km [6]. Therefore, despite the metamorphosed Permo-Triassic cover, the Kelebia basement area could not belong to this structural unit.

An Albian to Turonian age is generally proposed for the main deformation phase (D2) that forms the current geometry of the Alpine nappe stack [4–12]. The D2 phase led to a pervasive retrograde greenschist facies overprint in the structurally lower parts of the nappe pile. Additionally, the Codru Nappe System was also affected by the Turonian metamorphic overprint [6, 8]. Most likely, corresponding to the first significant Alpine orogenic event in the Tisza megaunit, the D2 phase resulted in the metamorphism of the prograde greenschist facies in the study area (Figure 11). This agrees with published mineralogical and geochronological data from wells in SE Hungary (basement high near Szeged and its surroundings), where the Alpine prograde metamorphism accompanied by mylonitization is attributed to Late Cretaceous Ar–Ar ages (mainly 96–82 Ma and somewhat younger) [55, 61, 62].

Furthermore, in the Apuseni Mountains, an approximately 30 km wide and more than 200 km long anastomosing Alpine crustal shear zone (Highiş–Biharia shear zone, HBSZ) was recognized along the boundary between the Tisza and Dacia megaunits that separates the Codru and Biharia Nappe Systems [8, 63]. Within the HBSZ, a minimum of 20 km of sinistral displacement was proposed, accompanied by phyllonite formation and an influx of fluid during greenschist to subgreenschist conditions. The lower part of the Biharia Nappe System was affected by repeated shearing events, and fluids were channeled by Alpine tectonic features [8, 63–65]. Additionally, it was suggested that the interval of the fractured crystalline basement rocks near Dorozsma (Do field, Figure 2) could be the western continuation of the HBSZ [25]. Based on the observed microtectonic indicators (e.g., fluid-related fringe structures, veinlets, FIPs, deformation lamellae in quartz, and fragmented porphyroclasts), we propose that the study area could belong to the abovementioned major shear zone, having both brittle and ductile segments. Consequently, the upper part of the Codru Nappe System, including the Permo-Triassic cover succession, was also affected by shearing episodes along the contact zone between the megaunits. It seems to be reasonable that the HBSZ could be dissected

during the Miocene extension of the Pannonian Basin, so different deeply buried segments of the shear zone could be expanded and moved away from each other at some distance.

Cretaceous tectonic elements could be easily reactivated during the Neogene rift-related extension, establishing structural control on fluid migration into fractured basement reservoirs. After the Middle Miocene, an intensive subsidence of the basement (mesogenesis II) resulted in the deposition of a thick (up to 4 km) sedimentary succession in the study area. The generation of HCs and the charging of the reservoirs occurred from the Late Miocene (or Pliocene) to the present-day [21, 25].

4. Conclusions

This case study highlights the major effects of diagenetic to metamorphic overprint on the mineralogy and micropetrographic features of three Permo-Triassic lithologies (Permian siliciclastics and ignimbrites, as well as Triassic sandstones) located in the pre-Cenozoic basement, Codru Nappe System (Szeged Basin, Hungary). The following conclusions can be drawn about the studied basement rocks:

- (1) Mineralogical and petrological data suggest that the Permo-Triassic noncarbonate cover succession in the Kelebia basement area suffered a high anchizonal to epizonal metamorphic alteration after their deposition. Additionally, several deformation features were recognized in the studied samples, showing a weakly to moderately developed disjunctive foliation in the Permian rocks
- (2) The occurrence of deformation lamellae in quartz overgrowth cement together with quartz veinlets and FIPs in Lower Triassic quartz arenite clasts indicates that the time of ductile and brittle deformation and contemporaneous fluid migration was before the Early Miocene partial surface exposure
- (3) Most likely, Cretaceous orogenic events favored the prograde reaction series of phyllosilicates (~300°C temperature for the peak metamorphism), instead of the depth of burial. We propose that the “Turonian” phase (Early–Late Cretaceous nappe stacking) resulted in the prograde greenschist facies metamorphism in the study area. Furthermore, the Permo-Triassic cover succession of the Codru Nappe System was also affected by shearing episodes along the contact zone between the Tisza and Dacia megaunits

The results provided here are an example of how knowledge of clay mineralogical and complex petrographic investigations can improve the interpretation of the tectonometamorphic evolution of a deeply buried orogen.

Data Availability

The mineralogical and petrographic data used to support the findings of this study are included within the article.

Conflicts of Interest

The authors declare that there is no conflict of interest regarding the publication of this paper.

Acknowledgments

This work was financially supported by the University of Szeged Open Access Fund (4635), the Bolyai Research Scholarship of the Hungarian Academy of Sciences (BO/266/18), and the National Research, Development, and Innovation Fund (projects no. K 108375 and K 131690). The authors would like to thank Tivadar M. Tóth (head of the Department of Mineralogy, Geochemistry and Petrology, University of Szeged) and Balázs Kiss (MOL Plc, Algyő) for providing the core material and thin-section collections that were essential for the research.

Supplementary Materials

Figure S1: generalized tectonic stratigraphy of the northern Apuseni Mountains [20]. Abbreviations: P: Permian; Tr: Triassic; J: Jurassic; K: Cretaceous. Figure S2: thin-section photomicrographs of the Permian ignimbrites, Kelebia area: alteration and deformation textures (a–e: well Kel–7 core #8, f: well Kel–23 core #3). (a) Deformation lamellae in a resorbed and fractured quartz phenocryst. (b, c) Domino-type and mosaic fragmented quartz crystals. Notice rotated quartz chips that flake off from the original fractured grains. (d, e) White mica strain shadow around an apatite grain. (f) Disjunctive foliation in a deformed ignimbrite sample (the trend of the cleavage domains is indicated by the yellow line). Notice mantled quartz clasts with strain shadows associated with strain caps. Abbreviations: PPL: plane-polarized light; XPL: cross-polarized light; Ap: apatite; Bt: biotite; Dol: dolomite; Ms: muscovite; Qz: quartz. Figure S3: thin-section photomicrographs of the Lower Triassic sandstones (well Móra–1 core #17). (a–d) Framework grains with quartz overgrowths. Quartz overgrowth cement postdated by silica (b) and carbonate (c) replacements. Note: thick ($>1\ \mu\text{m}$) deformation twins in carbonate. The appearance of tiny quartz veinlets (d) and transgranular microcracks is a characteristic feature. Abbreviations: XPL: cross-polarized light; Cb: carbonate; Lv: volcanic lithic fragment; Qm: monocrystalline quartz; Qp: polycrystalline quartz; Qz: quartz. Figure S4: thin-section photomicrographs of the representative clast types of the Lower Miocene conglomerate (well Ás–É–4 core #3). Abbreviations: PPL: plane-polarized light; XPL: cross-polarized light; FIP: fluid inclusion plain; Lm: metamorphic lithic fragment; Lm(s): metasedimentary lithic fragment (quartzite); Ls: sedimentary lithic fragment (dolomite); Lv: volcanic lithic fragment; Qm: monocrystalline quartz; Qp: polycrystalline quartz; Bt: biotite; Ms: muscovite; Ser: sericite; Qz: quartz. (*Supplementary Materials*)

References

- [1] L. Fodor, L. Csontos, G. Bada, I. Györfi, and L. Benkovics, “Cenozoic tectonic evolution of the Pannonian basin system and neighbouring orogens: a new synthesis of paleostress data,” in *The Mediterranean Basins: Tertiary Extension within the Alpine Orogen*, B. Durand, L. Jolivet, L. F. Horváth, and M. Séranne, Eds., vol. 156, pp. 295–334, Geological Society of London, 1999.
- [2] G. Tari, P. Dövényi, I. Dunkl et al., “Lithospheric structure of the Pannonian basin derived from seismic, gravity and geothermal data,” in *The Mediterranean Basins: Tertiary Extension within the Alpine Orogen*, B. Durand, L. Jolivet, L. F. Horváth, and M. Séranne, Eds., vol. 156, pp. 215–250, Geological Society of London, 1999.
- [3] L. Csontos and A. Vörös, “Mesozoic plate tectonic reconstruction of the Carpathian region,” *Palaeogeography, Palaeoclimatology, Palaeoecology*, vol. 210, no. 1, pp. 1–56, 2004.
- [4] L. Maženco and D. Radivojević, “On the formation and evolution of the Pannonian basin: constraints derived from the structure of the junction area between the Carpathians and Dinarides,” *Tectonics*, vol. 31, no. 6, 2012.
- [5] S. Merten, L. Maženco, J. P. T. Foeken, and P. A. M. Andriessen, “Toward understanding the post-collisional evolution of an orogen influenced by convergence at adjacent plate margins: Late Cretaceous-Tertiary thermotectonic history of the Apuseni Mountains,” *Tectonics*, vol. 30, no. 6, 2011.
- [6] A. Kounov and S. M. Schmid, “Fission-track constraints on the thermal and tectonic evolution of the Apuseni Mountains (Romania),” *International Journal of Earth Sciences*, vol. 102, no. 1, pp. 207–233, 2013.
- [7] F. Horváth, B. Musitz, A. Balázs et al., “Evolution of the Pannonian basin and its geothermal resources,” *Geothermics*, vol. 53, pp. 328–352, 2015.
- [8] M. K. Reiser, R. Schuster, R. Spikings, P. Tropper, and B. Fügenschuh, “From nappe stacking to exhumation: Cretaceous tectonics in the Apuseni Mountains (Romania),” *International Journal of Earth Sciences*, vol. 106, no. 2, pp. 659–685, 2017.
- [9] M. K. Reiser, G. Săbău, E. Negulescu, R. Schuster, P. Tropper, and B. Fügenschuh, “Post-Variscan metamorphism in the Apuseni and Rodna Mountains (Romania): evidence from Sm–Nd garnet and U–Th–Pb monazite dating,” *Swiss Journal of Geosciences*, vol. 112, no. 1, pp. 101–120, 2019.
- [10] L. Fodor, “Results, problems and future tasks of palaeostress and fault-slip analyses in the Pannonian basin: the Hungarian contribution,” *Földtani Közlöny*, vol. 149, no. 4, pp. 297–326, 2019.
- [11] S. Kovács, J. Haas, G. Császár, T. Szederkényi, G. Buda, and A. Nagymarosy, “Tectonostratigraphic terranes in the pre-Neogene basement of the Hungarian part of the Pannonian area,” *Acta Geologica Hungarica*, vol. 43, no. 3, pp. 225–328, 2000.
- [12] S. M. Schmid, D. Bernoulli, B. Fügenschuh et al., “The Alpine–Carpathian–Dinaridic orogenic system: correlation and evolution of tectonic units,” *Swiss Journal of Geosciences*, vol. 101, no. 1, pp. 139–183, 2008.
- [13] K. Ustaszewski, S. M. Schmid, B. Fügenschuh, M. Tischler, E. Kissling, and W. Spakman, “A map-view restoration of the Alpine–Carpathian–Dinaridic system for the Early Miocene,” *Swiss Journal of Geosciences*, vol. 101, no. S1, pp. 273–294, 2008.
- [14] J. Haas, T. Budai, L. Csontos, L. Fodor, and G. Konrád, *Pre-Cenozoic Geological Map of Hungary 1:500 000*, Hungarian Geological Institute, Budapest, 2010.
- [15] S. Kovács, K. Brezsnýánszky, J. Haas, and T. Szederkényi, “Tectonostratigraphic terrane and palaeoenvironment maps of the Circum-Pannonian region,” *Földtani Közlöny*, vol. 141, pp. 123–140, 2011.

- [16] J. Haas, T. Budai, L. Csontos, L. Fodor, K. Gyula, and B. Koroknai, "Geology of the pre-Cenozoic basement of Hungary," in *Explanatory notes for "Pre-Cenozoic geological map of Hungary" (1:500 000)*, Geological and Geophysical Institute of Hungary, Budapest, 2014.
- [17] S. M. Schmid, B. Fügenschuh, A. Kounov et al., "Tectonic units of the Alpine collision zone between eastern Alps and western Turkey," *Gondwana Research*, vol. 78, pp. 308–374, 2020.
- [18] K. Fintor and A. Varga, "Paleofluid fingerprint as an independent paleogeographic correlation tool: an example from Pennsylvanian sandstones and neighboring crystalline rocks (Tisia Composite Terrane, S Hungary)," *Geofluids*, vol. 2020, Article ID 3568986, 24 pages, 2020.
- [19] J. Haas and C. Péró, "Mesozoic evolution of the Tisza mega-unit," *International Journal of Earth Sciences*, vol. 93, no. 2, pp. 297–313, 2004.
- [20] I. Balintoni, C. Balica, M. Cliveți et al., "The emplacement age of the Muntele Mare Variscan granite (Apuseni Mountains, Romania)," *Geologica Carpathica*, vol. 60, no. 6, pp. 495–504, 2009.
- [21] I. Garaguly, A. Varga, B. Raucsik, F. Schubert, G. Czuppon, and R. Frei, "Pervasive early diagenetic dolomitization, subsequent hydrothermal alteration, and late stage hydrocarbon accumulation in a Middle Triassic carbonate sequence (Szegeed basin, SE Hungary)," *Marine and Petroleum Geology*, vol. 98, pp. 270–290, 2018.
- [22] G. Tari and F. Horváth, "Alpine evolution and hydrocarbon geology of the Pannonian basin: an overview," in *The Carpathians and their Foreland: Geology and Hydrocarbon Resources*, AAPG Memoir, vol. 84, J. Golonka and F. Picha, Eds., pp. 605–618, AAPG (The American Association of Petroleum Geologists), 2006.
- [23] B. Badics and I. Vető, "Source rocks and petroleum systems in the Hungarian part of the Pannonian basin: the potential for shale gas and shale oil plays," *Marine and Petroleum Geology*, vol. 31, no. 1, pp. 53–69, 2012.
- [24] E. Babinszki, M. Bauer, T. Budai et al., *Hydrocarbons in Hungary, Results and Opportunities*, Hungarian Energy and Public Utility Regulatory Authority, Budapest, 2018.
- [25] T. M. Tóth and I. Vargáné Tóth, "Lithologically controlled behaviour of the Dorozsma metamorphic hydrocarbon reservoir (Pannonian basin, SE Hungary)," *Journal of Petroleum Science and Engineering*, vol. 195, no. 107748, p. 6, 2020.
- [26] M. Szemerédi, R. Lukács, A. Varga et al., "Permian felsic volcanic rocks in the Pannonian basin (Hungary): new petrographic, geochemical, and geochronological results," *International Journal of Earth Sciences*, vol. 109, no. 1, pp. 101–125, 2020.
- [27] D. M. Moore and R. C. Reynolds, *X-Ray Diffraction and the Identification and Analysis of Clay Minerals*, Oxford University Press, Oxford, United Kingdom, 1997.
- [28] L. N. Warr and A. H. N. Rice, "Interlaboratory standardization and calibration of clay mineral crystallinity and crystallite size data," *Journal of Metamorphic Geology*, vol. 12, no. 2, pp. 141–152, 1994.
- [29] L. N. Warr and R. F. Mählmann, "Recommendations for Kübler index standardization," *Clay Minerals*, vol. 50, no. 3, pp. 283–286, 2015.
- [30] E. Mészáros, A. Varga, B. Raucsik, Z. Benkó, A. Heincz, and C. A. Hauzenberger, "Provenance and Variscan low-grade regional metamorphism recorded in slates from the basement of the (SW Hungary)," *International Journal of Earth Sciences*, vol. 108, no. 5, pp. 1571–1593, 2019.
- [31] M. Frey and E. Niggli, "Margarite, an important rock-forming mineral in regionally metamorphosed low-grade rocks," *Die Naturwissenschaften*, vol. 59, no. 5, pp. 214–215, 1972.
- [32] P. Árkai, K. J. T. Livi, M. Frey, A. Brukner-Wein, and C. Sajgó, "White micas with mixed interlayer occupancy: a possible cause of pitfalls in applying illite Kübler index ("crystallinity") for the determination of metamorphic grade," *European Journal of Mineralogy*, vol. 16, no. 3, pp. 469–482, 2004.
- [33] W. R. Dickinson, "Interpreting detrital modes of grauwacke and arkose," *Journal of Sedimentary Petrology*, vol. 40, no. 2, pp. 695–707, 1970.
- [34] F. J. Pettijohn, P. E. Potter, and R. Siever, *Sand and Sandstone*, Springer-Verlag, New York, 1972.
- [35] C. W. Passchier and R. A. J. Trouw, *Microtectonics*, Springer Science & Business Media, Berlin, Heidelberg, 2005.
- [36] D. L. Whitney and B. W. Evans, "Abbreviations for names of rock-forming minerals," *American Mineralogist*, vol. 95, no. 1, pp. 185–187, 2010.
- [37] K. J. T. Livi, D. R. Veblen, J. M. Ferry, and M. Frey, "Evolution of 2:1 layered silicates in low-grade metamorphosed Liassic shales of Central Switzerland," *Journal of Metamorphic Geology*, vol. 15, no. 3, pp. 323–344, 1997.
- [38] J. Esquevin, "Influence de la composition chimique des illites sur leur cristallinité," *Bulletin du Centre de Recherches Pau. SNPA*, vol. 3, pp. 147–153, 1969.
- [39] B. Kübler and M. Jaboyedoff, "Illite crystallinity," *Earth and Planetary Science Letters*, vol. 331, no. 2, pp. 75–89, 2000.
- [40] C. E. Weaver, *Clays, Muds, and Shales*, Elsevier, Amsterdam, 1989.
- [41] M. Frey and D. Robinson, *Low-Grade Metamorphism*, Blackwell Science Publishing, Oxford, United Kingdom, 1999.
- [42] I. Abad, "Physical meaning and applications of the illite Kübler index: measuring reaction progress in low-grade metamorphism," in *Diagenesis and Low-Temperature Metamorphism. Theory, Methods and Regional Aspects*, F. Nieto and J. Jiménez-Millán, Eds., vol. 3, pp. 53–64, Seminarios de la Sociedad Espanola de Mineralogía, 2008.
- [43] P. Árkai, R. J. Merriman, B. Roberts, D. R. Peacor, and M. Tóth, "Crystallinity, crystallite size and lattice strain of illite-muscovite and chlorite: comparison of XRD and TEM data for diagenetic to epizonal pelites," *European Journal of Mineralogy*, vol. 8, no. 5, pp. 1119–1138, 1996.
- [44] M. E. van Zalinge, K. V. Cashman, and R. S. J. Sparks, "Causes of fragmented crystals in ignimbrites: a case study of the Cardones ignimbrite, Northern Chile," *Bulletin of Volcanology*, vol. 80, no. 3, pp. 1–15, 2018.
- [45] D. J. Barber, H. C. Heard, and H. R. Wenk, "Deformation of dolomite single crystals from 20–800 °C," *Physics and Chemistry of Minerals*, vol. 7, no. 6, pp. 271–286, 1981.
- [46] R. H. Vernon, *A Practical Guide to Rock Microstructure*, Cambridge University Press, 2004.
- [47] P. Árkai, "Phyllosilicates in very low-grade metamorphism: transformation to micas," in *Micas: Crystal Chemistry and Metamorphic Petrology*, A. Sassi, F. P. Thompson, and J. B. Guggenheim, Eds., vol. 46, pp. 463–478, Reviews in Mineralogy and Geochemistry, 2002.
- [48] M. D. Rodríguez-Ruiz, I. Abad, and M. J. Bentabol, "Permo-Triassic clastic rocks from the Ghomaride complex and Federico units (Rif Cordillera, N Morocco): an example of

- diagenetic-metamorphic transition,” *Minerals*, vol. 9, no. 12, p. 738, 2019.
- [49] T. Blenkinsop, *Deformation Microstructures and Mechanisms in Minerals and Rocks*, Kluwer Academic Publishers, 2002.
- [50] M. G. C. Vernooij and F. Langenhorst, “Experimental reproduction of tectonic deformation lamellae in quartz and comparison to shock-induced planar deformation features,” *Meteoritics & Planetary Science*, vol. 40, no. 9-10, pp. 1353–1361, 2005.
- [51] J. Götze, M. Plötze, and D. Habermann, “Origin, spectral characteristics and practical applications of the cathodoluminescence (CL) of quartz – a review,” *Mineralogy and Petrology*, vol. 71, no. 3-4, pp. 225–250, 2001.
- [52] J. Sittner and J. Götze, “Cathodoluminescence (CL) characteristics of quartz from different metamorphic rocks within the Kaoko Belt (Namibia),” *Minerals*, vol. 8, no. 5, p. 190, 2018.
- [53] W. Hildreth and C. J. N. Wilson, “Compositional zoning of the bishop tuff,” *Journal of Petrology*, vol. 48, no. 5, pp. 951–999, 2007.
- [54] J. Wilcock, F. Goff, W. G. Minarik, and J. Stix, “Magmatic recharge during the formation and resurgence of the Valles Caldera, New Mexico, USA: evidence from quartz compositional zoning and geothermometry,” *Journal of Petrology*, vol. 54, no. 4, pp. 635–664, 2013.
- [55] P. Árkai, A. Bérczi-Makk, and K. Balogh, “Alpine low-T prograde metamorphism in the post-Variscan basement of the Great Plain, Tisza Unit (Pannonian basin, Hungary),” *Acta Geologica Hungarica*, vol. 43, no. 1, pp. 43–63, 2000.
- [56] R. Kemenci and M. Čanović, “Geologic setting of the pre-Tertiary basement in Vojvodina (Yugoslavia), part I: the Tisza Mega-unit of North Vojvodina,” *Acta Geologica Hungarica*, vol. 40, no. 1, pp. 1–36, 1997.
- [57] R. H. Worden and S. D. Burley, “Sandstone diagenesis: the evolution of sand to stone,” in *Sandstone Diagenesis: Recent and Ancient, Reprint Series vol. 4 of the International Association of Sedimentologists*, S. D. Burley and R. H. Worden, Eds., pp. 3–44, Blackwell Publishing, 2003.
- [58] C. Spötl and J. K. Pitman, “Saddle (baroque) dolomite in carbonates and sandstones: a reappraisal of a burial-diagenetic concept,” in *Carbonate Cementation in Sandstones*, S. Morad, Ed., vol. 26, pp. 437–460, International Association of Sedimentologists, 1998.
- [59] R. H. Worden and S. Morad, “Quartz cementation in oil field sandstones: a review of the key controversies,” in *Quartz Cementation in Sandstones*, R. H. Worden and S. Morad, Eds., vol. 29, pp. 1–20, International Association of Sedimentologists, 2000.
- [60] P. Árkai, K. Balogh, A. Demény, I. Fórizs, G. Nagy, and Z. Máthé, “Composition, diagenetic and post-diagenetic alterations of a possible radioactive waste repository site: the Boda Albitic Claystone Formation, southern Hungary,” *Acta Geologica Hungarica*, vol. 43, no. 4, pp. 351–378, 2000.
- [61] P. Árkai, “Alpine regional metamorphism in the main tectonic units of Hungary: a review,” *Acta Geologica Hungarica*, vol. 44, no. 2–3, pp. 329–344, 2001.
- [62] G. Lelkes-Felvári, W. Frank, and R. Schuster, “Geochronological constraints of the Variscan, Permian-Triassic and eo-Alpine (Cretaceous) evolution of the Great Hungarian Plain basement,” *Geologica Carpathica*, vol. 54, no. 5, pp. 267–280, 2003.
- [63] D. I. Pană and P. Erdmer, “Alpine crustal shear zones and pre-alpine basement terranes in the Romanian Carpathians and Apuseni Mountains,” *Geology*, vol. 22, no. 9, pp. 807–810, 1994.
- [64] B. Bonin and M. Tatu, “Cl-rich hydrous mafic mineral assemblages in the Highiş massif, Apuseni Mountains, Romania,” *Mineralogy and Petrology*, vol. 110, no. 4, pp. 447–469, 2016.
- [65] C. L. Ciobanu, N. J. Cook, F. Damian, and G. Damian, “Gold scavenged by bismuth melts: an example from Alpine shear-remobilizates in the Highiş Massif, Romania,” *Mineralogy and Petrology*, vol. 87, no. 3-4, pp. 351–384, 2006.

Supplementary Materials

Pre-Alpine terranes and their basement	Alpine metamorphosed cover of the pre-Alpine terranes		Alpine tectonic units		
Baia de Arieș terrane Baia de Arieș metamorphic sequence	<i>No metamorphic cover</i>		Highiș–Muncel Nappe Paiușeni sequence		Biharia Nappe System
			Baia de Arieș Nappe Baia de Arieș sequence		
Biharia terrane Biharia metamorphic sequence	Paiușeni Permian sequence	Vulturese–Belioara-Triassic marbles	Biharia Nappe Paiușeni sequence Vulturese-Belioara marbles Biharia sequence		Biharia Nappe System
			Poiana Nappe Paiușeni sequence		
			Arieșeni Nappe	P–Tr Paiușeni sequence Biharia sequence	
Someș terrane Someș metamorphic sequence	<i>No metamorphic cover</i>		Gârda Nappe	P–Tr Someș sequence	Codru Nappe System
			Colești Nappe	Tr–J	
			Vășcau Nappe	Tr–J	
			Moma Nappe	P–Tr	
			Dieva Nappe	P–K ₁	
			Finiș Nappe	P–K ₁ Someș sequence	
			Vălanii Nappe	Tr–K ₁	
			Bihor Unit	P–K ₁ Someș sequence	Bihor A.U.

Figure S1: Generalized tectonic stratigraphy of the northern Apuseni Mountains [20]. Abbreviations: P = Permian; Tr = Triassic; J = Jurassic; K = Cretaceous.

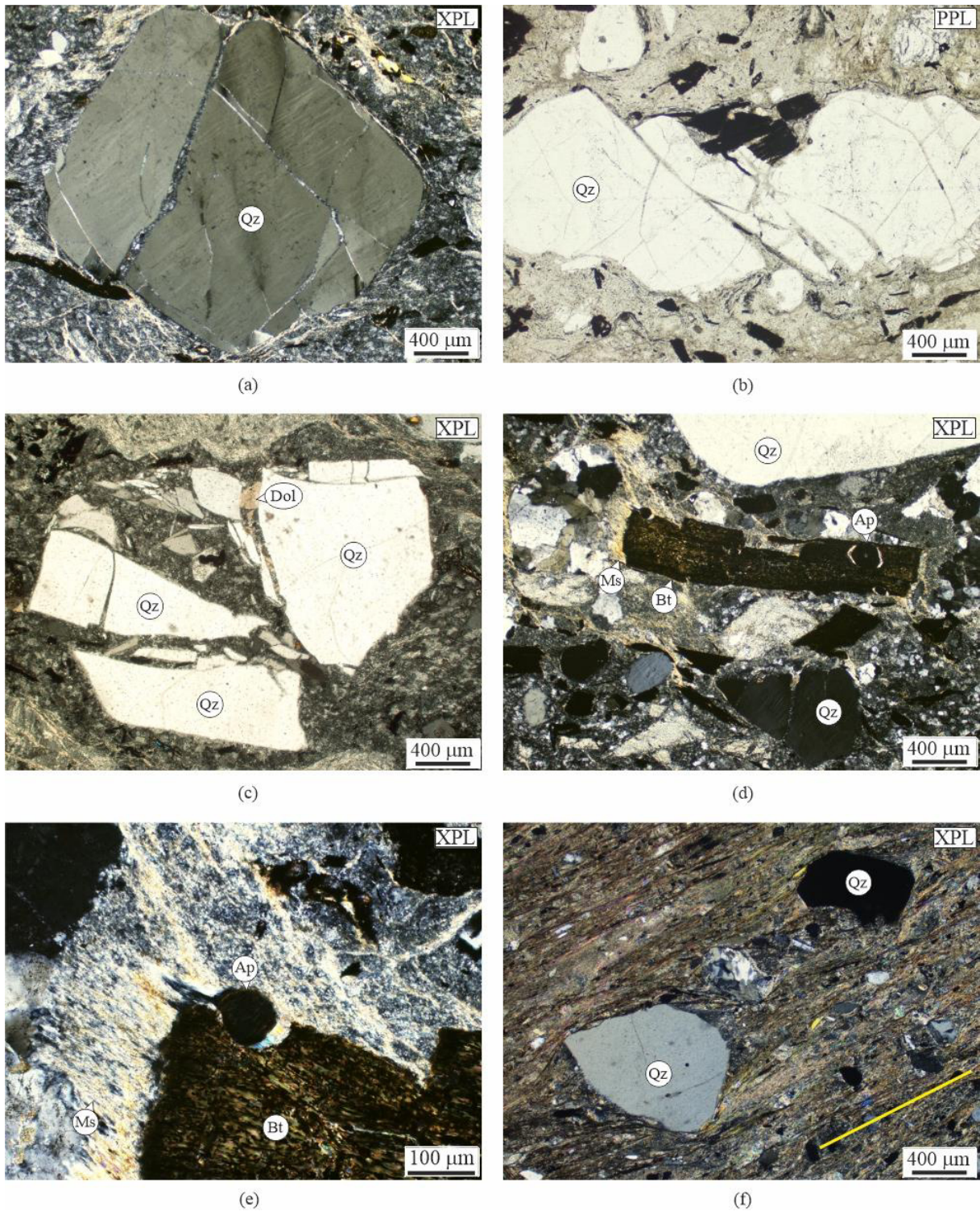
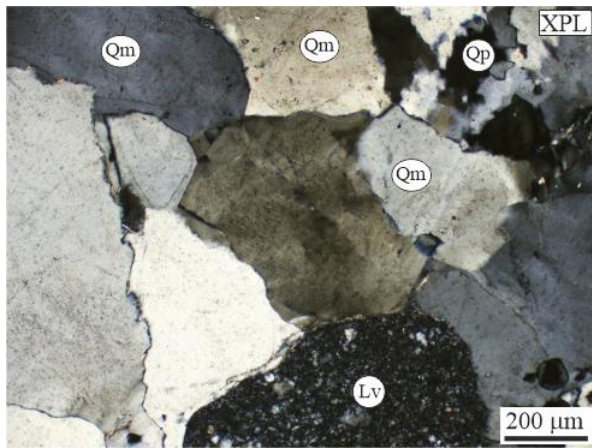
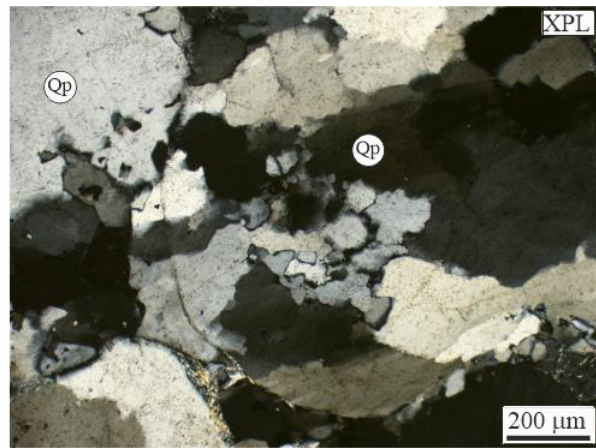


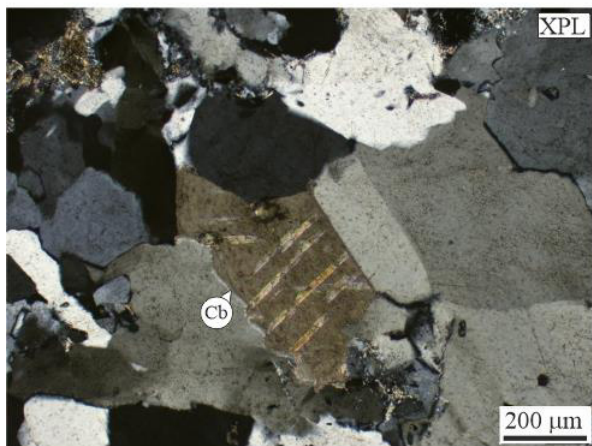
Figure S2: Thin-section photomicrographs of the Permian ignimbrites, Kelebia area: alteration and deformation textures (a–e: well Kel–7 core #8; f: well Kel–23 core #3). (a) Deformation lamellae in a resorbed and fractured quartz phenocryst; (b) and (c) Domino-type and mosaic fragmented quartz crystals. Notice rotated quartz chips that flake off from the original fractured grains; (d) and (e) White mica strain shadow around an apatite grain; (f) Disjunctive foliation in a deformed ignimbrite sample (the trend of the cleavage domains is indicated by the yellow line). Notice mantled quartz clasts with strain shadows associated with strain caps. Abbreviations: PPL = plane-polarized light; XPL = cross-polarized light; Ap = apatite; Bt = biotite; Dol = dolomite; Ms = muscovite; Qz = quartz.



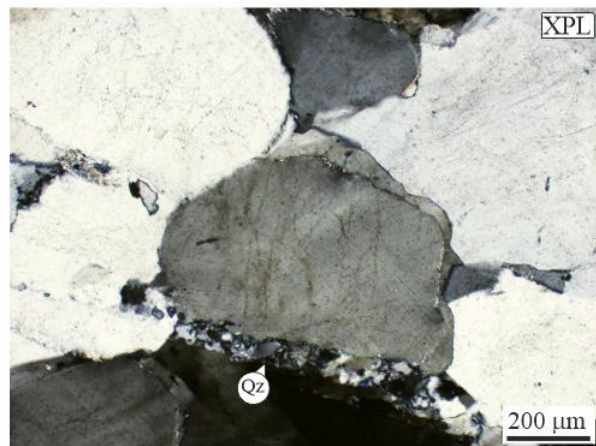
(a)



(b)



(c)



(d)

Figure S3: Thin-section photomicrographs of the Lower Triassic sandstones (well Móra-1 core #17); (a)–(d) Framework grains with quartz overgrowths. Quartz overgrowth cement postdated by silica (b) and carbonate (c) replacements. Note: Thick ($> 1 \mu\text{m}$) deformation twins in carbonate. The appearance of tiny quartz veinlets (d) and transgranular microcracks is a characteristic feature. Abbreviations: XPL = cross-polarized light; Cb = carbonate; Lv = volcanic lithic fragment; Qm = monocrystalline quartz; Qp = polycrystalline quartz; Qz = quartz.

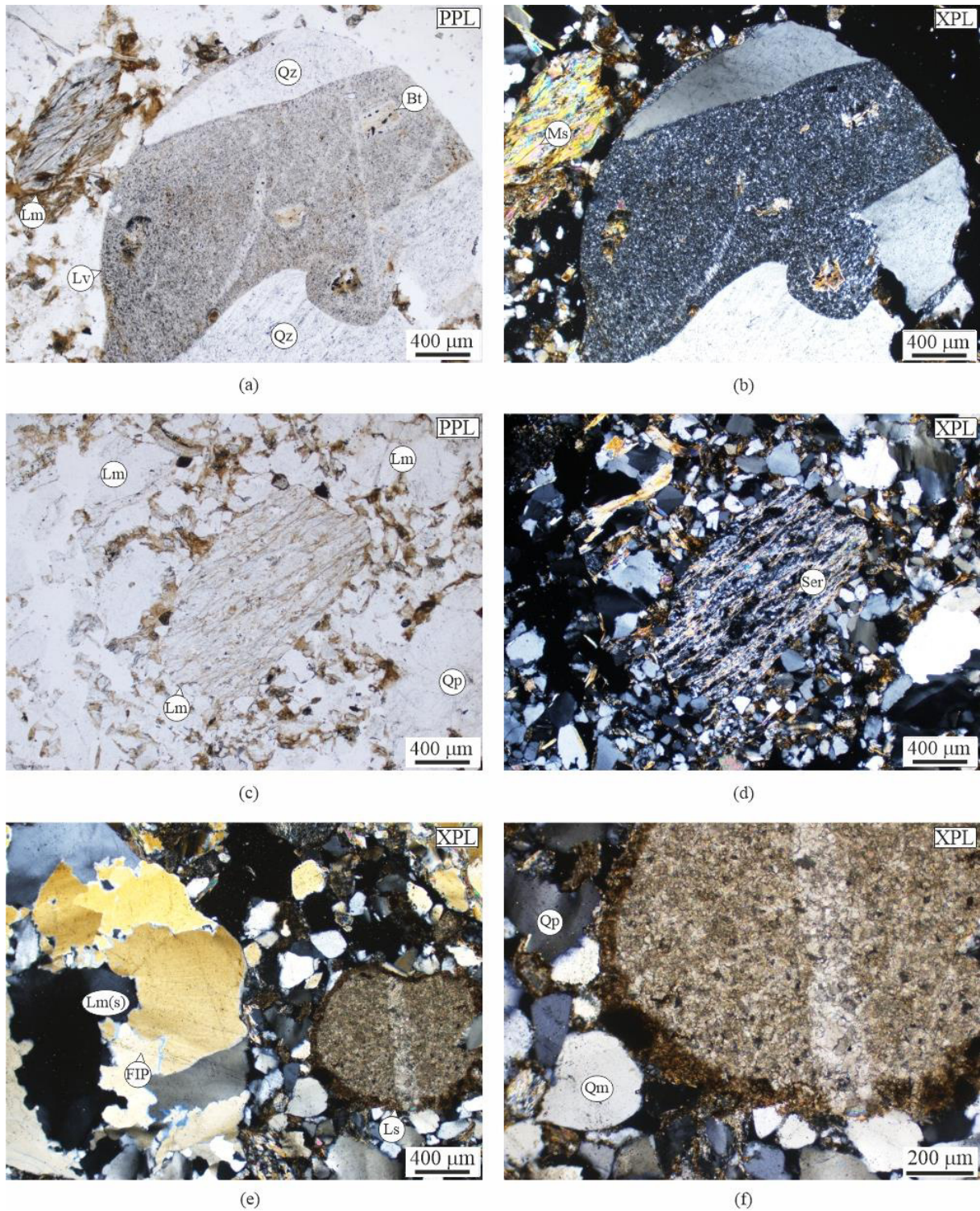


Figure S4: Thin-section photomicrographs of the representative clast types of the Lower Miocene conglomerate (well Ås-É-4 core #3). Abbreviations: PPL = plane-polarized light; XPL = cross-polarized light; FIP = fluid inclusion plain; Lm = metamorphic lithic fragment; Lm(s) = metasedimentary lithic fragment (quartzite); Ls = sedimentary lithic fragment (dolomite); Lv = volcanic lithic fragment; Qm = monocrystalline quartz; Qp = polycrystalline quartz; Bt = biotite; Ms = muscovite; Ser = sericite; Qz = quartz.